Phenomenology of squeezing and sliding of molecularly thin Xe, CH$_4$ and C$_{16}$H$_{34}$ lubrication films between smooth and rough curved solid surfaces with long-range elasticity

B. N. J. Persson[a]
IFF, FZ-Jülich, 52425 Jülich, Germany

V. N. Samoilov
IFF, FZ-Jülich, 52425 Jülich, Germany, and Physics Faculty, Moscow State University, 117234 Moscow, Russia

S. Zilberman
School of Chemistry, Tel Aviv University, Tel Aviv 69978, Israel and IFF, FZ-Jülich, 52425 Jülich, Germany

A. Nitzan
School of Chemistry, Tel Aviv University, Tel-Aviv 69978, Israel

The properties of Xe, CH$_4$ and C$_{16}$H$_{34}$ lubricant confined between two approaching solids are investigated by a model that accounts for the curvature and elastic properties of the solid surfaces. We consider both smooth surfaces, and surfaces with short-scale roughness. In most cases we observe well defined molecular layers develop in the lubricant film when the width of the film is of the order of a few atomic diameters, but in some cases atomic scale roughness inhibit the formation of these layers, and the lubricant exhibit liquid-like properties. An external squeezing-pressure induces discontinuous, thermally activated changes in the number n of lubricant layers. We observe that the layering transition tends to nucleate in disordered or imperfect regions in the lubrication film. We also present and discuss results of sliding dynamics for Xe and C$_{16}$H$_{34}$ lubrication films. © *2002 American Institute of Physics.* [DOI: 10.1063/1.1491888]

I. INTRODUCTION

Sliding friction is one of the oldest problems in physics, and has undoubtedly huge practical importance.[1] In recent years, the ability to produce durable low-friction surfaces and lubricant fluids has become an important factor in the miniaturization of moving components in technologically advanced devices. For those applications, the interest is focused on the stability under pressure of thin lubricant films, since the complete squeeze out of the lubricant from an interface may give rise to cold-welded junctions, resulting in high friction and catastrophically large wear.

Recently, a large number of computer simulations and analytical studies of simple models have been presented, with the aim to gain insight into the atomistic origin of sliding friction. Most computer simulations have used flat surfaces (with one important exception, Ref. 2), represented by thin (5–20 Å) solid layers, which could not account for long range elastic effects (see, e.g., Ref. 3). However, all experiments related to boundary lubrication and sliding friction measured the properties of curved surfaces of mesoscopic or macroscopic dimensions, for which the elastic response to external forces is an essential feature. For example, in the Surface Forces Apparatus,[4–6] very thin mica sheets are glued onto two cylindrical glass rods. By bringing the cylinders (rotated by 90° degrees relative to each other) in contact, a common interface is formed, whose shape and size is determined by the elastic deformation of the two solids. Curved surfaces are, of course, also involved in almost every real life sliding system, since even nominally flat surfaces have defects and asperities, and the contact between two macroscopic bodies will always occur in a number of discrete areas (typically of micrometer size). For very smooth surfaces, the asperities will mainly deform elastically, i.e., negligible plastic deformation will occur.

We note that in surface forces apparatus (SFA), and also in atomic force microscopy (AFM) studies the sliding velocity is usually much lower (of order 0.01–100 μm/s) than in most practical applications. In such applications, however, it is of fundamental importance to understand how fluids respond to severe and sudden changes of the environment. Thus, it often happens that fluids sustain the ultrafast and transient alteration of pressure, deformation rate or film thickness. We do not yet have good ways of thinking about how fluids respond to a severe change of environment that might last for a tiny fraction of a second. Some aspects of this short-time response of liquids and confined fluids can be probed using computer simulations. A good understanding of such computer "experiments," done for model systems characterized by different (realistic) parameters, may lead to a better understanding of the dynamics of thin confined liquid films and of boundary lubrication.

In this work we consider such a model system that takes

[a]Electronic mail: b.persson@fz-juelich.de

into account the effect of *long range elasticity* in the confining solids, and we apply it to study boundary lubrication for *curved solid surfaces*. In particular, we investigate the squeezing of molecular thin Xe, CH_4 (methane) and $C_{16}H_{34}$ (hexadecane) lubrication films, focusing on the nature of the $n \rightarrow n-1$ layering transitions (where n is the number of layers of lubrication atoms between the solid surfaces), that occur with increasing applied pressure. We also study the influence of short-wavelength surface roughness on the squeezing dynamics. In two earlier publications one of us has used the same model and presented results of squeezing and sliding with Xe as the boundary lubricant.[7,8] It is important to note that the qualitative picture that emerges from these simulations is valid for almost every solid interface, even if no lubricant has been intentionally added, since most real surfaces are covered by organic contaminants which have an effect very similar to that of added lubricants.

In the case of two curved elastic surfaces, the lubricant in the region of closest approach is in contact with the low pressure ''reservoirs'' that correspond to the regions with larger separation. With increasing pressure the width of the lubricant film in the regions of closest approach is reduced by discontinuous steps, corresponding to the reduction in the number of two dimensional (2D) lubricant layers at the interface. The elimination of each layer starts with the nucleation of a 2D void, which progressively grows by ejecting atoms into the low pressure regions.[7,9–11,12] We have shown earlier that the void formation is a thermally activated process, which, for 2D liquid-like layers, can be described by concepts borrowed from classical nucleation theory.[9]

In many practical situations the nucleation of the layering transition may occur at some ''weak'' point between the surfaces where imperfections, e.g., foreign adsorbates (like water or some organic contamination), may locally reduce the spreading pressure. The latter can even become negative, i.e., nonwetting. This has been observed in some experiments where the layering transitions start repeatedly at the same point in the contact area.[13] Similarly, in our computer simulations for $C_{16}H_{34}$ and Xe presented below we observe that if the tip of the block-asperity is centered over a disordered region in the lubrication film, the squeeze out nucleates at a lower pressure than when it is centered over a well ordered region. This situation is obviously similar to that for three-dimensional systems, where the formation of a new phase, e.g., solidification of an undercooled liquid, usually starts at ''impurities'' or at other anomalous points, such as dust particles, ions, surfaces, etc.

The assumption of a 2D liquid-like state for the lubricant layer is often not justified in practice, as indicated by a non-vanishing static friction force measured at most interfaces. Instead, the lubrication film is partly or entirely in a solid-like state, which can be either commensurate or incommensurate with the solid walls, and sometimes it is in a glassy state. Earlier simulations using Xe as a lubricant have shown that even for solid-like lubrication films, the thinning of the interface occurs in steps, and the layering transition starts by the nucleation of a small ''hole'' (stress aided activated process).[7] However, the squeeze-out kinetics depends on the precise state of the lubricant layers. For flat solid surfaces

separated by unpinned or weakly pinned (incommensurate) lubrication layers, fast and complete layering transitions usually occur. Commensurate or strongly pinned incommensurate layers lead to sluggish and incomplete transitions, possibly leaving islands trapped in the contact region. In fact, for commensurate layers we observe that it is nearly impossible to squeeze-out the last few layers simply by increasing the perpendicular pressure. However, the squeeze-out rate is enhanced by lateral sliding, since, in this case, the lubricant film can turn into a disordered or fluid-like state, facilitating the ejection of an entire layer.

In this study we consider the late stages of the approach of two solid surfaces, wetted by Xe, CH_4 or $C_{16}H_{34}$ lubricants, and forming a curved interface. Our simulation reproduces the step-like evolution of the parameters characterizing the interface, corresponding to the discontinuous change in the number n of lubricant layers in the region of shortest separation. We discuss in detail the nature of the nucleation of the squeeze-out of the last two layers of lubrication molecules.

II. MODEL

Our model was described in Ref. 7, and we review it briefly here. We are concerned with the properties of a lubricant film squeezed between the curved surfaces of two elastic solids. In experiments, a system of this type is obtained by gluing two elastic slabs (of thickness W_1 and W_2) to ''rigid'' surface profiles of arbitrary shape. If the radius of curvatures of the rigid surfaces are large compared to W_1 and W_2, the elastic slabs will deform, reproducing with their free surfaces the (nearly arbitrary) shape of the underlying rigid profiles.

In what follows we denote the lower solid as *substrate*, which is taken to be fixed in space. The upper solid, denoted as *block*, will be moving. To account for the elastic response of the slabs, without dealing with the large number of atoms required to simulate a mesoscopic elastic solid we treat explicitly, at the atomistic level, only the last atomic layer of the solids at the interface. These atoms are connected to a *rigid* curved surface (or profile) of mass M. The force constants connecting these atoms to the rigid profile, however, are not the bare parameters, determined by the model interatomic potential. Instead, those force constants are treated as effective parameters that implicitly re-introduce the elastic response of the slabs of arbitrary width W_1 and W_2.

The model is illustrated in Fig. 1 (see also Ref. 7). The atoms in the bottom layer of the block (open circles) form a simple square lattice with lattice constant a, and lateral dimensions $L_x = N_x a$ and $L_y = N_y a$. In the following, periodic boundary conditions are assumed in the xy plane. The atoms interact with each other via ''stiff'' springs (thick lines) and execute bending and stretching motion characterized by a bending force constant k_{0B} and a stretching force constant k_0, respectively. Moreover, each atom is connected to the upper rigid surface profile by ''soft'' elastic springs, of bending force constant k_{1B} and stretching force constant k_1. The numerical value of all these force constants k_0, k_{0B}, k_1 and k_{1B} are determined in such a way as to mimic the elastic
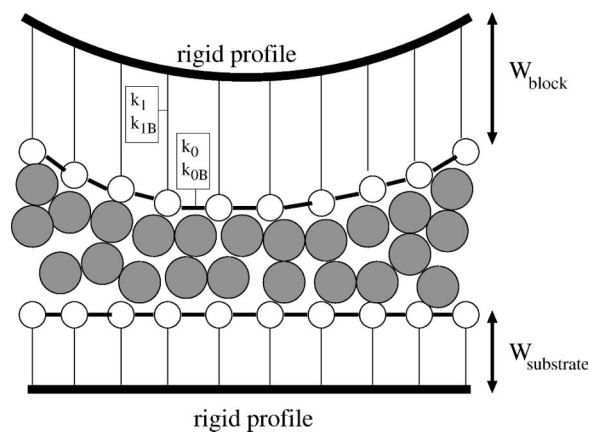
FIG. 1. Schematic picture of the central region of the squeezing model in the present article.
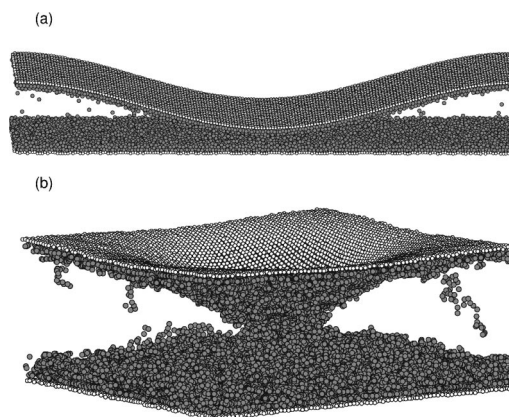

FIG. 2. Snapshot pictures of the two system geometries studied in the present paper. The bottom surface of the block atoms and the top layer of the substrate atoms and the lubrication atoms or molecules are indicated. (a) Cosine corrugated block (in the x-direction) with lateral size 640 Å (in the x-direction) and 96 Å (in the y-direction) lubricated by Xe atoms. (b) Gaussian asperity-block with lateral size 200 Å $\times$ 200 Å lubricated by $C_{16}H_{34}$.

response of the entire slab. If we apply a shear stress σ to the slab, the resulting strain ϵ is given by $\sigma = 2G\epsilon$, where $G = E/2(1+\nu)$ is the shear modulus, E is the elastic modulus and ν the Poisson ratio. If we write the shear strain as $\epsilon = \Delta/2a$ then $\sigma = k_{0B}\Delta/a^2 = G\Delta/a$ and we get $k_{0B} = Ga$. Similarly, we obtain that $k_0 = Ea$. Next, let us consider an elastic slab of thickness W. If we apply a shear stress σ, we get the relative displacement x so that the strain is $\epsilon = x/2W$. Thus $\sigma = Gx/W$ which must equal $k_{1B}x/a^2$ and hence $k_{1B} = Ga^2/W$. In a similar way one can obtain $k_1 = Ea^2/W$.

The substrate is treated in a similar way as the block, but we use slightly different lattice constants in order to avoid having (low order) commensurate structures formed at the interface. The space between the block and the substrate is occupied by a layer (monolayer or more) of the lubrication fluid.

The MD-calculations have been performed by keeping the temperature of the solid wall fixed at their outer boundaries (see Ref. 7). This is a realistic treatment, and it implies that heat flow from the lubricant to the confining walls.

Below we study the pressure both at the center of the contact area, and the average pressure. The pressure acting on a wall atom is defined as the total normal force acting on the wall atom from the lubricant atoms and from the other wall, devided by the area a^2. The average pressure is the z-component of the total normal force acting on the solid block from the lubricant and the substrate, divided by the total area $L_x \times L_y$.

In the following subsections we provide details of the models used for the block, the substrate and the lubricants in the different simulations carried in the present work.

A. Block and substrate

The block and substrate are characterized by the number of of atoms N_x and N_y in the x and y directions, respectively, and the lattice constant a (square lattice is assumed). The choice of a should be consistent with the mass density ρ of the solids, which were either steel or gold. However, to avoid commensurability between the block and the substrate surfaces, we have taken their lattice constants slightly different from each other.

The elastic properties of the solids are determined by the Poisson ratio ν, the elastic Young modulus E [which is related to the shear modulus $G = E/2(1+\nu)$]. From these quantities and the thickness W, we determine the spring constants k_0, k_{0B}, k_1 and k_{1B} defined above. In all the simulations described below we have used the same elastic moduli and Poisson ratio for the block and substrate, which were $E = 1 \times 10^{11}$ Pa and $\nu = 0.3$ for "steel," and $E = 7.72 \times 10^{10}$ Pa and $\nu = 0.42$ for the "gold." However, we have used different choices of W for the block and substrate. The substrate is only one monolayer thick $W \approx a$, while the block was assigned a width $W = 100$ Å. These choices of thicknesses imply that the block used in our simulations will deform elastically much more then the substrate.

For the Xe simulations we have used a system of lateral dimensions $L_x = 640$ Å, $L_y = 96$ Å. The block had a mass $M = 10^6$ atomic units, and the hard profile was taken to be cosine corrugated in the x direction, with corrugation amplitude $0.1L_x$ and wavelength L_x. The substrate was flat with $N_x = 200$ and $N_y = 30$ atoms in the x and y directions, with lattice constant $a = 3.2$ Å. The corresponding parameters for the block were $N_x = 180$ and $N_y = 27$ and $a = 3.56$ Å. Figure 2(a) shows a simulation snapshot that demonstrates the cosine corrugation.

In the simulations with CH_4 and $C_{16}H_{34}$ the solid walls had elastic properties corresponding to gold with the lateral dimensions $L_x = L_y = 200$ Å. For the substrate we used $N_x = N_y = 79$ atoms in the x and y directions, forming a square lattice with lattice constant $a = 2.53$ Å. The corresponding parameters for the block are $N_x = N_y = 73$, $a = 2.74$ Å. In the simulations the rigid surface had a mass $M = 10^6$ atomic units, and Gaussian corrugation of height and width equal to 40 Å [see Fig. 2(b)]. We also used two types of substrate corrugations—atomically flat surfaces and "nanocorrugated" surfaces. In the later case the rigid substrate profile had a sine corrugation of the form

$$h(x,y)=h_0 \sin\left(\frac{2\pi x}{\lambda}\right)\sin\left(\frac{2\pi y}{\lambda}\right), \tag{1}$$

with roughness amplitude $h_0=3$ Å and $h_0=1.5$ Å for simulations with CH_4 and $C_{16}H_{34}$ lubricants, respectively, and the wavelength $\lambda=0.1L_x$. Thus we studied the effect of a single wavelength nano-roughness on the confined lubricant structure and dynamics.

B. Lubricants

Two models for atomic lubricants and one model for chain lubricant were employed. Lennard-Jones potentials were used for the atomic lubricants to model the interactions between lubricant atoms:

$$v(r)=4\epsilon_0\left[\left(\frac{r_0}{r}\right)^{12}-\left(\frac{r_0}{r}\right)^{6}\right], \tag{2}$$

and the same potential with modified parameters (ϵ_1, r_1) were used for the interaction with the block and substrate atoms.

For the Xe–Xe interaction $\epsilon_0=20$ meV and $r_0=4$ Å, and for the Xe–wall atom interaction $\epsilon_1=60$ meV and $r_1=4.4$ Å. The latter choice reflects the stronger interaction between Xe and a metal surface.

The second atomic model was CH_4 (methane) in the united atom representation. We used $\epsilon_0=12.75$ meV and $r_0=3.73$ Å [14] for the interaction between the CH_4 molecules, and $\epsilon_1=18.60$ meV and $r_1=3.28$ Å for the CH_4–block and the CH_4–substrate interaction. [15]

In order to be able to examine similarities and differences between simple atomic species and more complex lubricants, we have also used a model of hexadecane $C_{16}H_{34}$, as a prototype chain molecule. We used chains of 16 beads in a united atom representation. The interaction between each bead and the block/substrate atoms were taken the same as for CH_4. For the interactions within the $C_{16}H_{34}$ we have used the OPLS model (Refs. 14 and 16). The parameters for the interaction between the bead units on different lubricant molecules were $\epsilon_0=5.12$ meV for interior beads, $\epsilon_0=7.590$ MeV for end beads and $r_0=3.905$ Å in all cases. The usual combining rule was applied for bead–bead interaction $\epsilon_{ij}=\sqrt{\epsilon_i\epsilon_j}$. [17] Atomic mass 14 (for interior CH_2 beads) and 15 (for the CH_3 end groups) were used. For the bead–block and the bead–substrate interactions we took $\epsilon_1=18.60$ meV and $r_1=3.28$ Å. [15] Within a $C_{16}H_{34}$ chain we assume nearest neighbor C atoms are connected via springs with the spring constant k, which was chosen either equal to 10 or 45 N/m (both values gave similar results). Note that those values are one order of magnitude smaller then the optimized 450 N/m, [14] and were chosen such as to facilitate a reasonable time steps of 1–2 fs. We used an angle bending interaction of the form $E(\cos\theta)=1/2k_{bend}(\cos\theta-\cos\theta_0)$ with $k_{bend}=62543$ K and $\theta_0=2.0001$ rad. For the dihedral interaction we used the functional form in term of a cosine Fourier series $E(\phi)/k_B=\sum_{i=0}^{3}c_i\cos^i(\phi)$ with parameters $c_0=1009.99$ K, $c_1=2018.95$ K, $c_2=136.37$ K, $c_3=-3165.30$ K. Internal beads of separation greater than 3 units are treated similarly as beads from different chains.
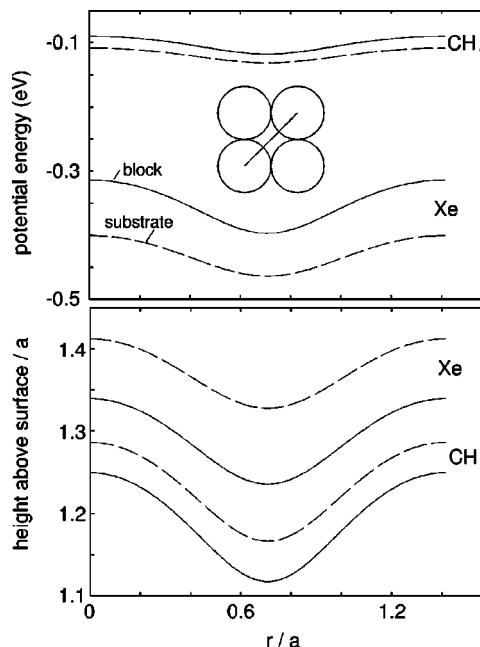

FIG. 3. (a) The potential energy and (b) the height above the surface of the minima, as a function of the lateral position of the Xe or CH_4 atom between the on-top to hollow to on-top site [see the inset of (a)]. Results are shown for Xe and CH_4 on the block and on the substrate surfaces. The height in (b) is normalized by the lattice constant of the block and the substrate, respectively. Solid and dashed lines refer to the interaction with the block and substrate, respectively.

C. Binding energies and squeeze velocities

Characteristic features of the molecule–surface interactions are displayed graphically in Fig. 3. Here r is the distance along a line connecting the on-top sites through a hollow position (in units of the substrate or block lattice constant). Figure 3(a) shows the variation of the potential energy, and Fig. 3(b) the distance of the adsorbate from the top layer (for the substrate) or bottom layer (for the block) of solid atoms, as the adsorbate is displaced along the ground state potential energy surface. The solid and dashed curves refer to the substrate and the block, respectively. They differ from each other because of the different lattice constants chosen for the substrate and the block. The binding is, as expected, strongest in the hollow sites and weakest in the on-top sites. Table I summarizes the binding interaction parameters for Xe and CH_4. For $C_{16}H_{34}$ we have used the same wall–$CH_{2,3}$ bead interaction as the wall–CH_4 interaction. We

TABLE I. Lubricant–solid binding characteristics; see also Fig. 3. E_B is the binding energy in the hollow site. The corrugation in the potential energy is the difference between its value in the on-top site and the value in the hollow site (in % of its hollow site value). The height modulation is the height difference (in units of the lattice constant a) between the on-top and hollow sites.

Molecule	E_B [eV]		Potential corrugation [%]		Height modulation [/a]	
	Block	Substrate	Block	Substrate	Block	Substrate
Xe	0.40	0.46	21	13	0.08	0.12
CH_n	0.118	0.131	23	18	0.13	0.10

note that when an adsorbate layer is confined at high pressure between two solid surfaces, the effective barrier for lateral diffusion will strongly increase.

For these different systems we ran simulations in which the block approaches the substrate with constant velocity v_z up to some distance. When we discuss the displacement d of the block, we refer to the motion of the rigid profile toward the substrate rigid profile, where the reference $d=0$ correspond to an (arbitrary) block–substrate separation chosen close to the initial contact. In the simulations with Xe we have studied both the approach and the retraction process, by reversing the motion direction of the block at the closest approach point. Next we describe our results.

The squeeze velocity we use (~ 1 m/s) is much higher than in most experiments, e.g., in SFA-experiments. However, from the point of view of many applications, the squeeze velocity ~ 1 m/s is not particularly high. Thus, computer simulations are complementary to SFA measurements. Nevertheless, we believe that the qualitative picture we obtain from our simulations is valid also at low squeeze velocity, although the nucleation of squeeze-out will occur at a lower applied pressure when the squeezing velocity is reduced, since we have shown earlier that it is a (stress-aided) thermally activated process (see Ref. 7). The squeeze-out (after nucleation) often occur very rapidly when the contact area is small (as in computer simulations); thus, during squeeze-out, the squeeze velocity is often unimportant (e.g., the upper surface of the solid block has often moved a negligible distance during the squeeze-out time period).

III. SIMULATION RESULTS: SQUEEZING

In this section we describe the results obtained from our simulations for the three different lubricants, Xe, CH_4 and $C_{16}H_{34}$.

A. Xe lubricant

For the Xe simulations we have used 14,000 lubricant atoms between walls with elastic properties corresponding to steel (see Sec. II), at temperature $T=200$ K. Since the lattice constants of the substrate and the block ($a=3.2$ Å and 3.56 Å, respectively) are significantly smaller than the Xe–Xe equilibrium separation (which is close to $r_0=4$ Å) we expect, at least in the absence of a confining pressure, that the Xe layers adsorbed on the solid walls form hexagonal incommensurate structures, and that the adsorbate layers are only weakly pinned. However, when confined at high pressure between the solid walls we find (see below) that the Xe atoms on the block wall form a domain wall super structure with areas of 1×1 structure, separated by low-density domain walls.

The Xe lubricant is confined between the flat substrate surface and the cosine-corrugated block surface, and the block first moves toward the substrate with the velocity $v_z = 0.445$ m/s. At short block–substrate separation, when two monolayers of trapped Xe occur in the contact area at the interface, we reverse the velocity to -0.445 m/s.

Figure 4 shows (a) the dependence of the average pressure, and (b) the average Xe kinetic energy on the distance the upper surface of the block has moved toward the bottom
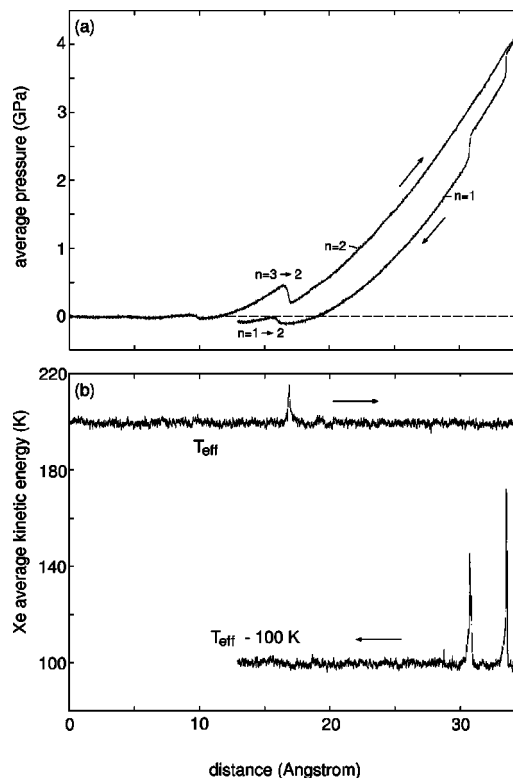

FIG. 4. The dependence of the average pressure (top) and the average Xe kinetic energy (bottom) on the distance the upper surface of the block has moved toward the bottom surface of the substrate (temperature $T=200$ K, and the squeeze velocity $v_z=0.445$ m/s). The squeezing is followed by retraction with the velocity $v_z=-0.445$ m/s.

surface of the substrate. Note that the x-axis is the displacement of the upper surface of the block, and *does not* represent the vertical separation between the block and the substrate. Initially (before contact) both surfaces are covered by about 2.5 monolayers of Xe. When the two solids are squeezed together a small flat contact region develops separated by an integer number of Xe layers. As the squeezing pressure increases, the individual layers are squeezed out in relatively rapid events. The squeeze-out events are separated by time intervals where mainly elastic loading occurs. The $n=3\rightarrow2$ squeeze-out event is seen in Fig. 4(a) as a rapid drop in the average pressure, and in Fig. 4(b) as a (small) kinetic energy spike. The transition from $n=2\rightarrow1$, which is completed during the retraction, turns out to be more complex and interesting, and we now discuss it in detail.

The $t=0$ snapshot picture in Fig. 5, from the central region of the contact area, shows the trapped bilayer of Xe at the distance ≈ 30 Å in Fig. 4. The picture is from top of the block, and for clarity we do not show the block and substrate atoms. At the periphery of the contact area the Xe atoms form hexagonal layers: this maximize the binding energy of Xe within the layer. However, in the central part of the contact region the Xe atoms form (relative to the block surface) a 1×1 domain wall super-structure, where the domain walls have a lower concentration of Xe atoms than in the perfect 1×1 structure. The origin of this phase transformation from hexagonal layers in the low pressure region to the domain–wall super-structure at the center is that the latter structure
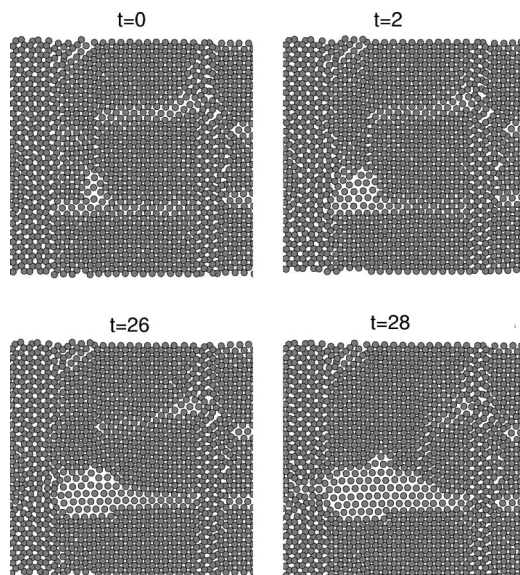
t=0   t=2

t=26   t=28

FIG. 5. Snapshot pictures during squeeze-out. The time is in natural units where $t=0$ correspond to a squeezing distance $d\approx30$ Å in Fig. 4. For the temperature $T=200$ K, and the squeeze velocity $v=0.445$ m/s.

allows the solid walls to approach each other by a small distance which gives rise to a lowering of the total energy since the elastic energy stored in the walls is reduced. We believe that phase transformations of this type are very common (a similar transformation occurs for the CH_4 lubricant studied below), although the exact structures formed will depend upon the system studied.

A similar phase transformation was discussed in detail in Ref. 7. The difference between the present case and Ref. 7 is that, because the lattice constant of the block in the present case is larger and more similar to the natural Xe–Xe separation, the system form a 1×1 domain wall structure rather than the $c(2\times2)$ layers formed in the study in Ref. 7, where the lattice constant of the block was the same as of the substrate (3.2 Å).

In Fig. 6 we show a snapshot picture of the same system as in Fig. 5 but including the atoms (unfilled circles) of the bottom surface of the block (and of the top atoms of the substrate): from this figure it is clear that the Xe atoms (in the high-pressure region) form commensurate 1×1 regions separated by low-density domain walls. In this case, however, since the lattice constant of the substrate is smaller than that of the block, the 1×1 regions are (nearly) incommensurate relative to the substrate. One consequence of this is that while the Xe film is strongly pinned to the bottom surface of the block, the pinning to the substrate is much weaker and during sliding one therefore expect the trapped bilayer to slide mainly relative to the substrate. The fact that the lubrication film is strongly pinned to the bottom surface of the block has profound implications for the squeeze-out dynamics. This differs from the case studied earlier, where the lattice constant of the block was the same as that of the substrate, and where the lubrication film in the high-pressure region formed a $c(2\times2)$ structure. This structure corresponds to a lower concentration of Xe atoms than the 1×1 structure formed in the present case. As a result, the nucle-
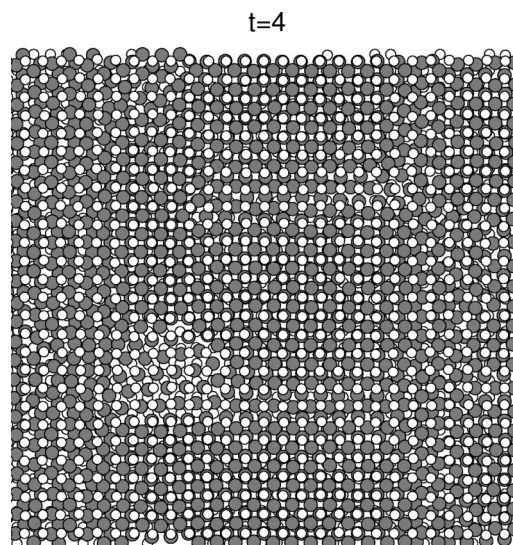
t=4

FIG. 6. Snapshot picture during squeeze-out. The white circles are the bottom layer of atoms on the block (the top layer of atoms of the substrate are also displayed but are mainly hidden by the Xe atoms). Note the formation of a domain wall super structure, where areas of 1×1 Xe structure are separated by low-density domain walls. However, the 1×1 Xe domains are (nearly) incommensurate with respect to the substrate top layer of atoms (not shown). The pictures correspond to a squeezing distance of about $d=30$ Å (the time $t=4$ refer to Fig. 5). For the temperature $T=200$ K, and the squeeze velocity $v=0.445$ m/s.

ation of the squeeze-out in the former case was easier, and the $n=2\rightarrow1$ squeeze-out was similar to that of the $n=3\rightarrow2$ transition, namely very fast and occurring in a single step, starting with the thermally activated formation of a small "hole" in the bilayer. In the present case the squeeze-out occurs stepwise in a series of fast events. The first event starts at $d\approx30$ Å and involves the formation of a small "hole" in the *region of a low-density domain wall* as indicated by the $t=2$ snapshot in Fig. 5. This hole remains for a short time period after which a rapid squeeze-out event occur along a low-density domain wall as illustrated in snapshot pictures $t=26$ and 28 in Fig. 5. This event is very similar to a crack propagating along a grain boundary in a solid and may have a similar physical origin, involving stress concentration at the crack tip. The system displayed in snapshot $t=28$ remains stable even when the average pressure increases to 4 GPa, which was the highest squeezing pressure in the simulation. The origin of this stability is the strong pinning (to the block surface) the Xe-layer experience. The lateral barrier which must be overcome to squeeze out the layer increases with the applied pressure. However, during the retraction we observe further squeeze-out, resulting in a (intermediate) state with a single monolayer of trapped Xe atoms. This latter squeeze-out occurred in two major events as illustrated in Fig. 4(a) by the two nearly vertical drops in the average pressure, and by the two Xe kinetic energy spikes in Fig. 4(b) during retraction. The $t=(60,80)$ and $t=(280,300)$ pair of snapshot pictures in Fig. 7 illustrate these two rapid events.

Figure 7 shows a larger part of the contact area than in Fig. 5 (the width in the y-direction is the same but the width in the x-direction is larger). The dark (fine grained) gray area

J. Chem. Phys., Vol. 117, No. 8, 22 August 2002
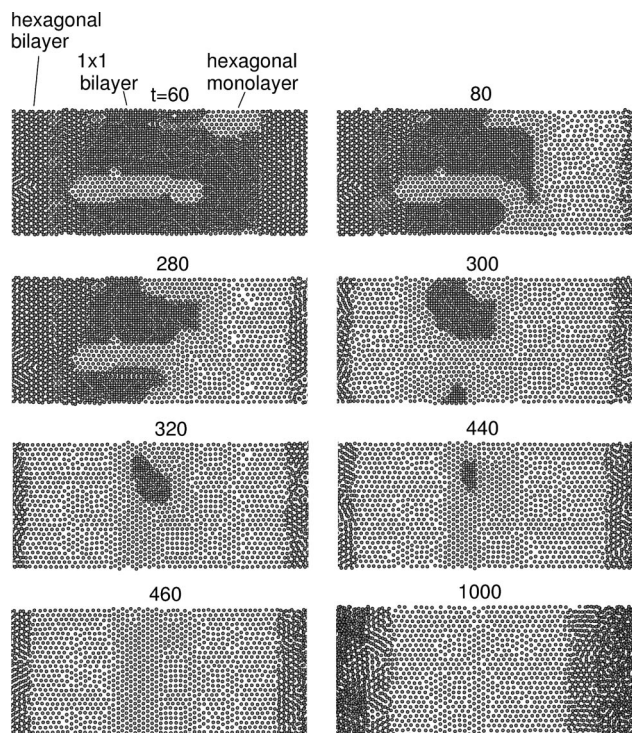
Phenomenology of squeezing and sliding   3903

FIG. 7. Snapshot pictures during retraction. $t=0$ correspond to the start of retraction. The retraction velocity is $v_z=-0.445$ m/s. These pictures show a larger part of the contact area than in Fig. 4 (the width in the y-direction is the same but the width in the x-direction is larger). The dark (fine grained) gray area is the (bilayer) 1×1 structure, while some hexagonal (bilayer) Xe structure can be observed at the periphery of the contact area in snapshot $t=60$, 80, and 280. The dotted area is the hexagonal Xe monolayer which remains after the $n=2\rightarrow1$ transition is completed.

FIG. 8. Capillary bridge formed during retraction at the velocity $v_z=-0.445$ m/s. $t=0$ corresponds to the last data point in Fig. 4.

is the (bilayer) 1×1 structure, while some hexagonal (bilayer) Xe structure can be observed at the periphery of the contact area in snapshot pictures $t=60,80$ and 280. The dotted (monolayer) area is the hexagonal Xe monolayer film which remains after the $n=2\rightarrow1$ transition is completed. We note that even though most of the bilayer disappears in the two rapid transitions $[t=(60,80)$ and $(280,300)]$ an island of 1×1 (bilayer) remains trapped for a while, and only gradually disappears as it is squeezed *into* the first monolayer. This process is accompanied by a lateral flow of atoms in the monolayer film toward the periphery of the contact area; the density of the monolayer film cannot increase very much because of the strong Xe–Xe repulsion at a short distance. The speed of the island squeeze-out is determined by the sliding friction as a patch of the Xe monolayer film slide relative to the solid walls. It is interesting to note that the local concentration of Xe atoms in the vicinity of the bilayer island is somewhat higher then farther away from it; thus, there must be a 2D pressure gradient in the monolayer film, which, of course, is the driving force of the lateral flow. During the flow this pressure gradient is mainly balanced by a frictional shear stress acting on the monolayer film as it slides or drifts relative to the solid walls.

Figure 4 shows that the monolayer film is stable during retraction until the average pressure becomes slightly negative (i.e., a pull-off force act on the block) at which point the (small strip) of monolayer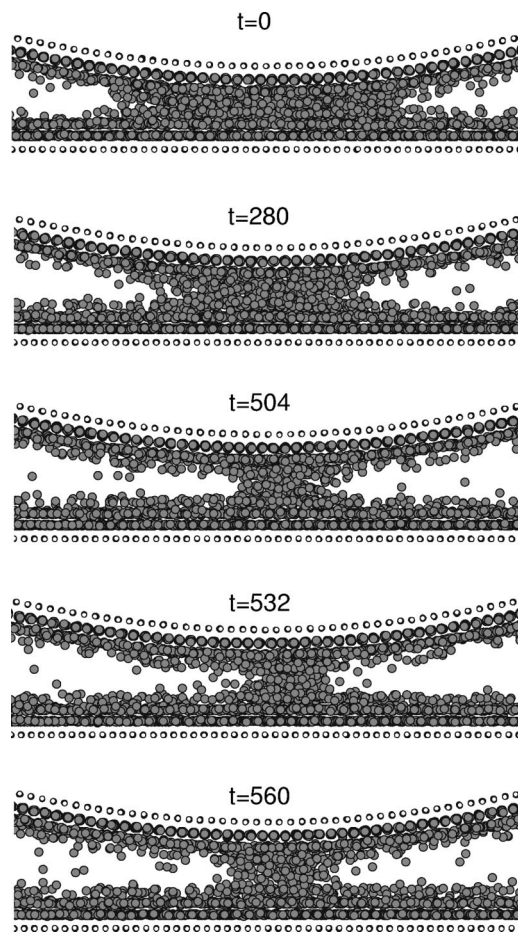 film (in a rapid event) thicken to two monolayers by the injection of a second Xe-layer at the interface. From here on the changes in the film between the solid walls is more sluggish and liquid-like, and when the solid walls are separated by more that 4 monolayers of Xe, snapshot pictures indicate the formation of a liquid-like Xe-bridge. This is illustrated in Fig. 8 which shows some snapshot pictures of the Xe-bridge which is formed during retraction of the block beyond the last data point in Fig. 4. Thus, the $t=0$ picture corresponds to the last point during retraction in Fig. 4, and the other snapshot pictures ($t>0$) correspond to later times not shown in Fig. 4. During retraction, the total displacement of the (upper surface) of the block between the $t=0$ and $t=560$ snapshot pictures is about 7.2 Å. The corresponding average pressure as a function of time is shown in Fig. 9. Note that the pull-off force drops by a factor ~6 during the full time period. This is in rough agreement with the Laplace theory of capillary pressure: $P_{\text{bridge}} = \gamma/r$ where r is the radius of curvature of the liquid meniscus and γ the surface tension of the liquid. According to this formula, the pull-off force is proportional to l_x/r, where l_x is the width of the capillary bridge. When going from $t=0$ to $t=560$ the width decreases from $l_x\approx25a$ to $9a$ (where a is the lattice constant of the block). To estimate the change in r we note that both solid surfaces have one monolayer of adsorbed Xe, which we assume is in a solid-like state, and which we therefore do not include when estimating the thick-
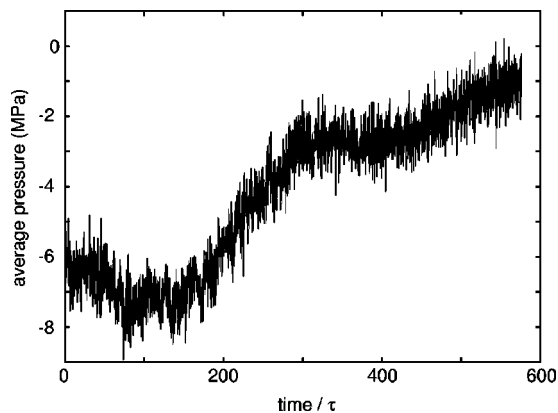
FIG. 9. The average pressure acting on the solid walls during retraction. Retraction velocity $v_z = -0.445$ m/s. The time $t=0$ corresponds to the last data point in Fig. 4.
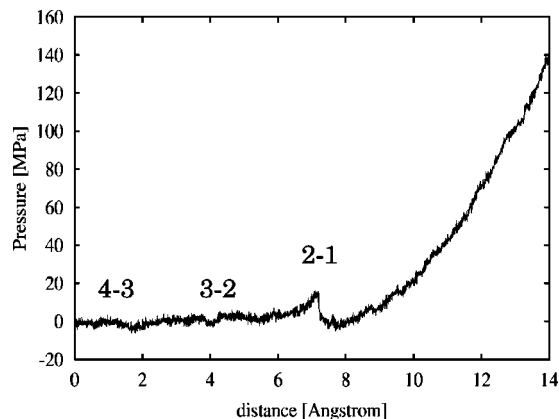

FIG. 10. The variation of the average pressure, as a function of the displacement of the upper surface of the block towards the (flat) substrate. The n-m labels stands for the layering transition from n to m layers. Squeezing velocity $v_z = 1$ m/s.

ness of the bridge. Using this approach, the radius of curvature increases from $r \approx 9$ Å to $r \approx 19$ Å. This gives a factor of $\sim (25/9)/(9/19) \approx 6$ drop in the pull-off force, in excellent agreement with the observation. The (negative) pressure in the bridge can be calculated using $P_{\text{bridge}} = P L_x / l_x$ where P is the average pressure. Thus, for the last snapshot picture in Fig. 8 where $P \approx -1$ MPa, $l_x \approx 9a$ and $L_x = 180a$, we get $P_{\text{bridge}} \approx -20$ MPa (corresponding roughly to -200 atm). This is in rough agreement with theory: Using the Laplace equation with $r \approx 19$ Å (see above) and the surface energy estimated using $\gamma \approx 3 n_0 \epsilon_0 / 2 \approx 2$ meV/Å^2, where $n_0 \approx 2/(r_0^2 \sqrt{3})$ is the surface coverage of Xe, we obtain the pressure $P_{\text{bridge}} = -17$ MPa, in rough agreement with the simulation. We note, however, that the (average) pressure in Fig. 9 does not decrease monotonically with time (or displacement). This indicates that the film is too thin to behave as a macroscopic (continuous) fluid. During elongation the bridge displays yield events, as typical for the plastic deformation of solids. Thus, the nanometer thick bridge, at the high strain rates probed in the calculations, has properties which are somewhere between those expected for solids and liquids.

B. CH$_4$ lubricant

We consider now the simulations with the CH$_4$ lubricant (in the united atom representation). In the simulations we use 10,000 atoms, confined between two gold-like surfaces: a flat substrate and a block with a Gaussian asperity. Since the binding energy of the CH$_4$ molecules to the solid surfaces is much smaller then in the Xe system, we have performed our studies at the temperature $T=100$ K.

Figure 10 shows the pressure variation as the upper surface of the block moves with the velocity $v_z = 1$ m/s towards the flat substrate. We show the average pressure as a function of the displacement of the upper surface towards the substrate. Note that we could not squeeze-out the last monolayer even when the (average) pressure is increased to 140 MPa. We now discuss in greater detail the observed layering transitions.

In the vicinity of the $n=4 \rightarrow 3$ layering transition, the overall pressure is slightly negative ($\sim 1-2$ MPa) due to a capillary bridge attraction. This is an indication of fluid-like

behavior. This assertion is further supported by the simulation snapshots (not shown) where we observe a disorderd fluid-like structure formed in the central contact region just prior to the squeeze-out.

Figure 11(a) is a magnification of Fig. 10, in the vicinity of the $n=3 \rightarrow 2$ layering transition. The first interesting feature is that even though the overall pressure grows linearly as the surfaces approach, the local pressure at the center is approximately constant [see Fig. 11(b)] up to the layering tran-
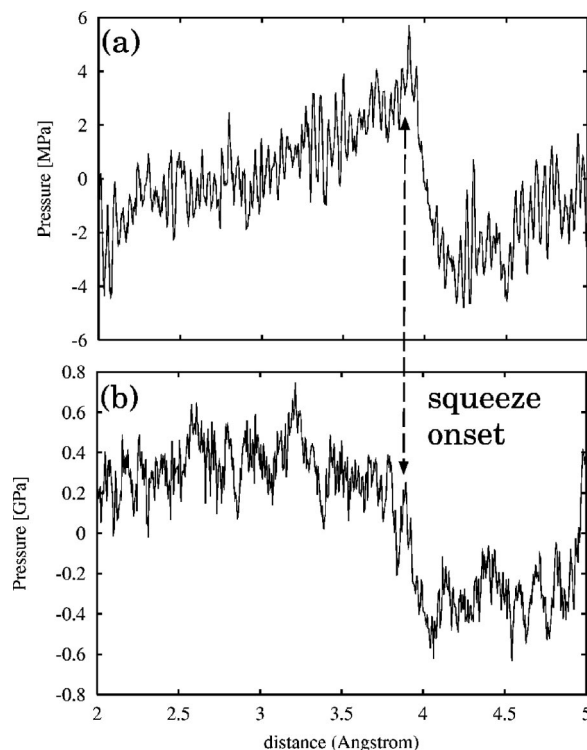

FIG. 11. The variation of (a) the average pressure, (b) the pressure at a specific central atom, as a function of the displacement of the upper surface of the block towards the (flat) substrate for the $n=3 \rightarrow 2$ transition. Squeezing velocity $v_z = 1$ m/s. This is a magnification of Fig. 10 in the vicinity of the $n=3 \rightarrow 2$ layering transition.
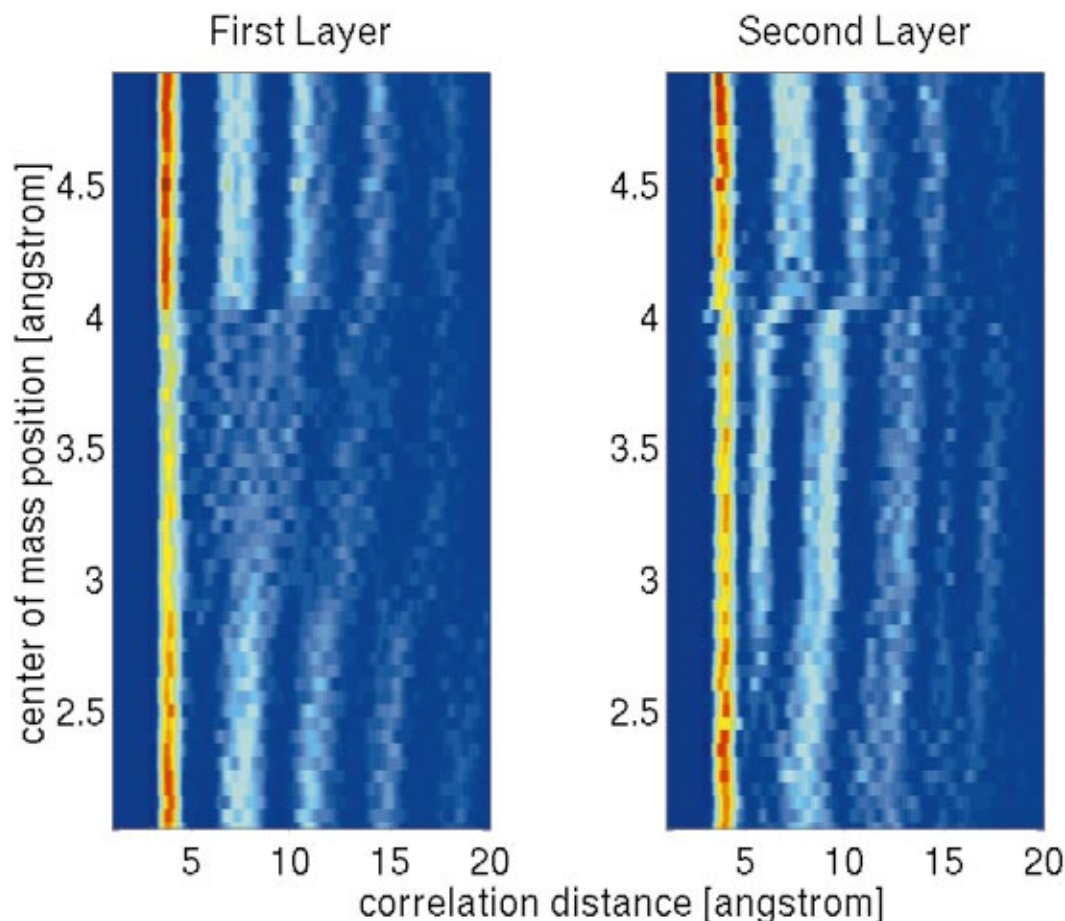
FIG. 12. (Color) The evolution of the in-plane pair correlation function, $g(r,d)$, at the contact area, as the block approaches the substrate in the vicinity of $n=3\rightarrow2$ layering transition. Here r (horizontal axis) is the correlation coordinate and d (vertical axis) is the distance the upper surface of the block has moved towards the substrate. The numerical value of g is highest at the red zones and lowest at the dark blue ones. The left figure corresponds to the first layer in contact with the substrate and the right figure to the second layer above.

sition point. We attribute it to local ''yielding'' (molecular rearrangement) of the confined lubricant in the central (high-pressure) region of the contact area.

Evidence for this yielding is obtained from the examination of structural data. Figure 12 shows the evolution of the in-plane pair correlation function,

$$g(r,d)=\frac{A}{N^2}\left\langle\sum_i\sum_{j\neq i}\delta(\mathbf{r}-\mathbf{r}_{ij})\right\rangle, \qquad (3)$$

for a section of area A (containing N atoms) in the center of the contact area, in the vicinity of the $n=3\rightarrow2$ layering transition. Here r (horizontal axis) is the correlation coordinate, and d (vertical axis) the distance by which the upper surface of the block has moved towards the substrate. The color scale denotes the magnitude of $g(r,d)$, where the highest magnitude corresponds to the red zones and lowest at the dark blue ones. The left figure corresponds to the first layer in contact with the substrate and the right figure to the second layer above. Note that we could not calculate $g(r,d)$ for the third layer which is in contact with the block, since its geometry was too curved, following that of the asperity. It is easily seen that prior to the layering transition, there is a continous restructering of the confined lubricant at the contact, which is related to the pressure yielding described

above. In particular it is interesting to observe that as the pressure increases there appears an additional peak in $g(r,d)$ of the second layer (indicating a change in the structure of the second layer), while peaks dissapear (or are blurred) in the first layer (indicating an increased dissorder within the first layer). This may indicate that the layering transition occurs by expulsion of the layer right next to the substrate.

A detailed analysis of the $n=2\rightarrow1$ transition (Fig. 13) reveals similar dynamics. The expulsion process is proceeded by a structural change (yield) which starts at the position of the pressure peak. By the time the squeeze-out starts (as indicated by the position of the arrow) the pressure is reduces roughly by a factor of two. Moreover, simulation snapshots (Fig. 14) also shows the formation of a more open structure during the yield, where the lubrication molecules in contact with the tip form a $c(2\times2)$ (approximately commensurate) structure and the second layer (in contact with the substrate) a similar structure, thus allowing the second layer to relax slightly towards the first layer, which relief elastic energy in the block. A similar effect was observed for the Xe-lubricant (see Sec. III A).

Figure 15 shows the evolution of the in-plane pair correlation function $g(r,d)$, at the contact area, in the vicinity of $n=2\rightarrow1$ layering transition (notations and color codes
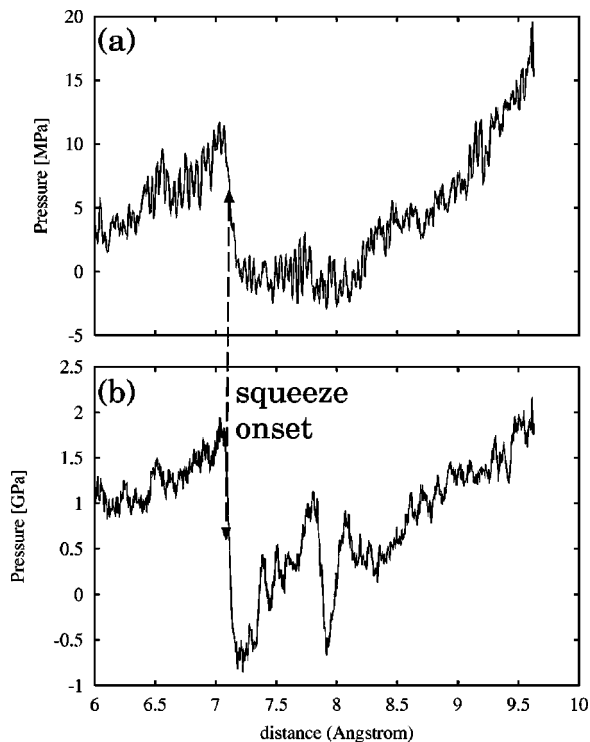
FIG. 13. The variation of (a) the average pressure and (b) the pressure at a specific central atom, as a function of the displacement of the upper surface of the block towards the (flat) substrate for the $n=2\rightarrow1$ transition. Squeezing velocity $v_z=1$ m/s. This is a magnification of Fig. 10 in the vicinity of the $n=2\rightarrow1$ layering transition. The layering transition does not start at the pressure peak, but rather at the point marked by the arrow (see the text).

FIG. 14. (Color) Snapshot pictures of the CH_4 atoms in the contact area during the "yield" or rearrangement transition preceeding the $n=2\rightarrow1$ layering transition (solid Au atoms are excluded). The figure shows the central $30\,\text{Å}\times30\,\text{Å}$ section (in the xy-plane) viewed from the substrate side. The color scheme represents the vertical z-coordinate, changing from dark blue at the first layer next to the substrate, to red far away. (a) shows the system just before the "yield" onset [indicated by the pressure peak in Fig. 13], and (b) just before the layering onset.

are the same as in Fig. 12). The left figure corresponds to the first layer in contact with the substrate and the right figure to the layer above it. Note that following the transition, the peaks in the correlation function of the first layer are significantly enhanced (and slightly shifted), indicating a greater degree of in-plane ordering. The inspection of the peak positions of the correlation function of the first layer, at distances corresponding to the snapshots of Fig. 14, shows that both the first and the second peak are shifted by 0.3–0.4 Å to greater in-plane separation between the atoms, supporting the yield–response (structural change) interpretation.

The final state of the squeeze-out is a nearly perfect commensurate (relative to the substrate) $c(2\times2)$ structure, shown in Fig. 16 from the direction of the substrate (with the top layer of substrate atoms included in the picture).

We now consider the effect of surface corrugation. Figure 17 is the analog of Fig. 10, where now the substrate is a corrugated (see Sec. II A). Again the block moves with velocity $v_z=1$ m/s towards the substrate, and we show (a) the average pressure and (b) the pressure at a specific atom at the center of the contact, as a function of the displacement of the upper surface of the block towards the substrate.[18]

There are some fundamental differences in the squeeze-out dynamics between the corrugated and the flat substrate cases: In the present case the fluid-like behavior extends down to all but the last monolayer, as manifested, e.g., by the negative pressure (associated with a capillary bridge) acting on the block up to a displacement ~5 Å; see Fig. 17(a). An
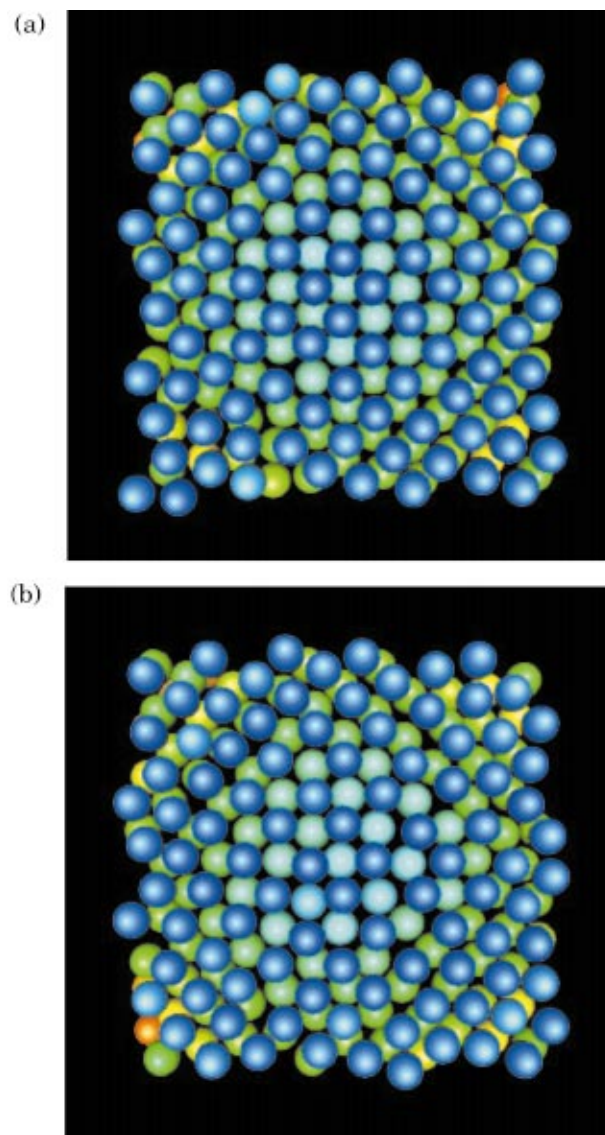
inspection of simulation snapshots (Figs. 18 and 19) also reveals a disordered state.

We also observe that the layering transitions in the rough substrate case occurs at much lower pressures compared to the flat substrate case. For example, the $n=2\rightarrow1$ transition occurred at average pressure of ~7 MPa for the rough surface compared to ~14 MPa for the flat one. We also manage to obtain a squeeze-out (though partial) of the last lubricant layer at a pressure of ~80 MPa, while for the flat case we could not squeeze it out even when the pressure was increased to 0.5 GPa (not shown here). The likely reason for this difference is that the rough substrate inhibits solidification (or ordering) of the lubricant under confinement, causing it to behave in a liquid-like viscoelastic manner.
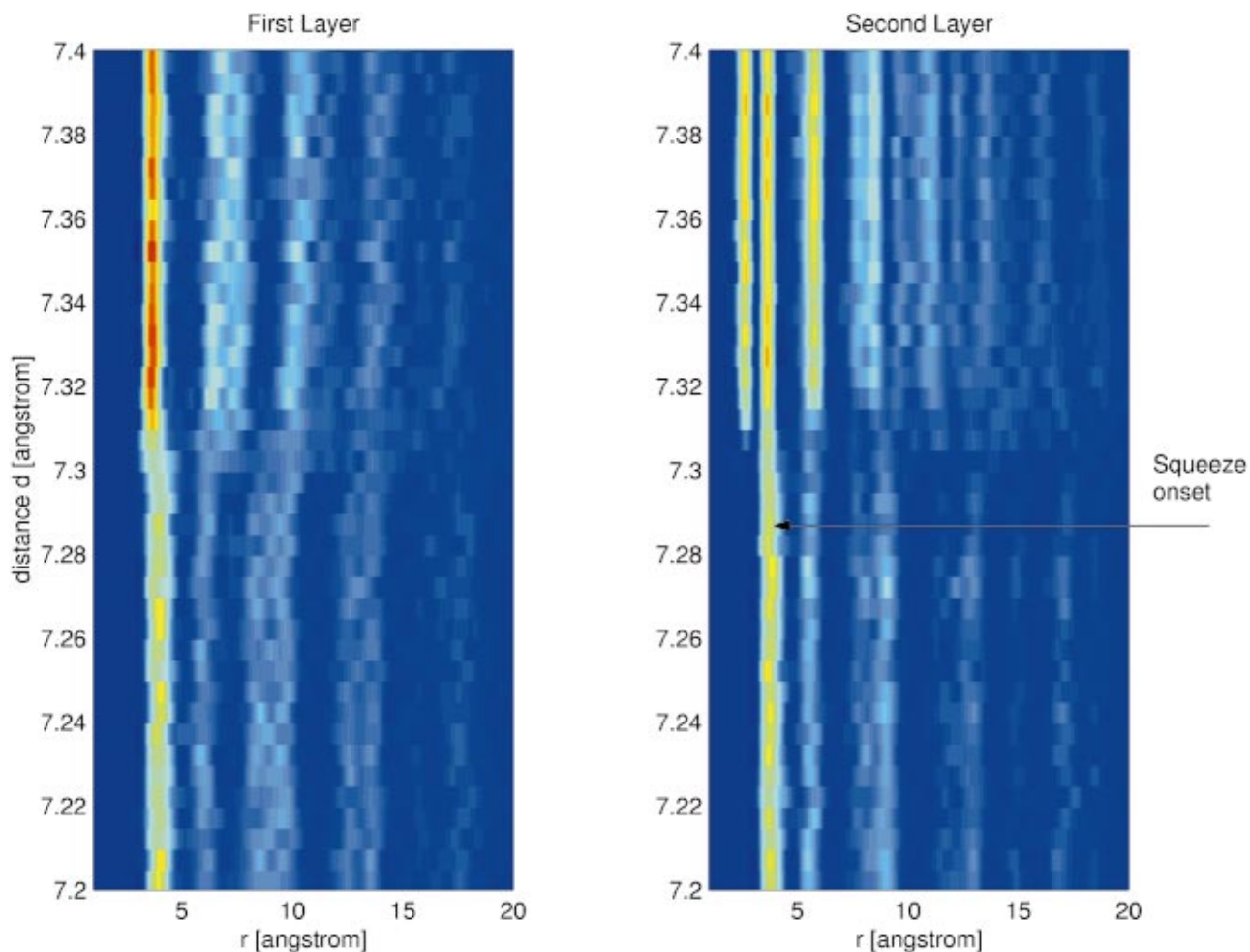
FIG. 15. (Color) The evolution of the in-plane pair correlation function, $g(r,d)$, at the contact area, in the vicinity of the $n=2\rightarrow1$ layering transition. Here r (horizontal axis) is the correlation coordinate and d (vertical axis) the distance the upper surface of the block has moved towards the substrate. The color intensity scale is highest at the red zones and lowest at the dark blue ones. Left: the layer closest the substrate. Right: the layer closest to the block. Note that well beyond the layering transition we have only a single confined lubricant layer, and the right figure shows essentially the structure of the solid asperity.

Figure 20 shows a snapshot where CH_4 molecules are trapped in the valleys generated by the surface roughness profile. Trapped fluid pockets were recently observed experimentally (but for flat surfaces) by Mugele and Salmeron[10] and analyzed by methods of continuum mechanics modeling in Refs. 11 and 12. We have also observed the trapping of lubrication fluid in surface roughness cavities for $C_{16}H_{34}$ (see below). We note that in some technological applications surface roughness cavities can have advantages in retaining lubricants, and for this reason an extremely low level of roughness may not always be necessary in, e.g., ball bearings.

C. $C_{16}H_{34}$ lubricant

Next we consider $C_{16}H_{34}$ as a prototype model of a chain lubricant. Our simulations were done with 2,000 $C_{16}H_{34}$ molecules (~5 monolayers) between the same solid walls as used for CH_4, at temperature $T=300$ K. The squeeze velocity was taken to be $v_z=2$ or 5 m/s. In the case of a corrugated substrate, the amplitude of the corrugation equals 3 Å instead of 6 Å as in the case of CH_4. Figure 21 shows the dependence of the average pressure on the block position as

it moves towards the substrate. Results are shown both for a smooth substrate, and for a substrate with short-wavelength corrugation. Note that the squeeze-out of the last monolayer occurs at much lower pressure for the corrugated substrate than for the flat substrate. However, in another simulation we found the opposite behavior, and a detailed study of snapshot pictures shows that the important factor is not the corrugation, but rather the nature of the lubrication film in the high-pressure region adjacent to the tip of the block. Thus, if the adsorbate layer is disordered in this region, or if the top of the tip is located in the region between two $C_{16}H_{34}$ domains (areas of aligned chains), then the squeeze-out nucleates at a lower pressure than when the top of the tip presses against the center of a well ordered $C_{16}H_{34}$ domain.

Figure 22 shows snapshot pictures taken close to the onset of the squeeze-out. Shown is the layer of the lubricant molecules adsorbed on the flat (left image) and the corrugated (right image) substrate surfaces used to obtain the results of Fig. 21. The top of the tip is located above the point where the two diagonal lines cross. Note that for the flat surface the tip is centered in the middle of a large $C_{16}H_{34}$ domain, while on the corrugated surface the tip is centered in
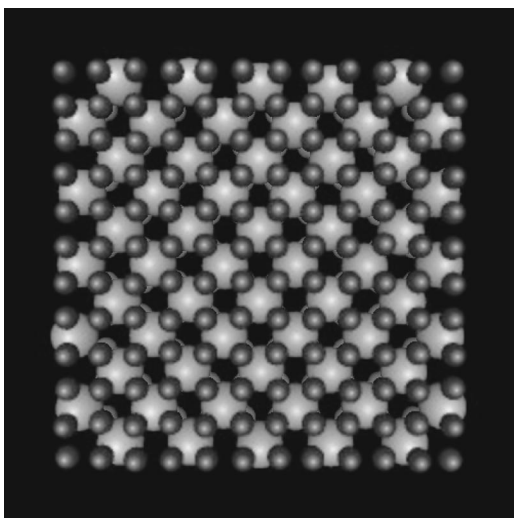
FIG. 16. Snapshot picture of the final system configuration for the squeeze-out of CH_4, with solid Au atoms included. The figure shows the central 30 Å×30 Å section (in the xy-plane) viewed from the substrate side. The gray scale represents the vertical z-coordinate, changing from dark gray at the substrates layer, to light gray far away.

a disordered region of the adsorbate layer. In most practical applications, the radius of curvature of the tip will be much larger than in the present study. In such cases one expect that the nucleation will occur in a ''weak point'' (e.g., disordered area) somewhere within the central part of the contact region where the pressure is highest.
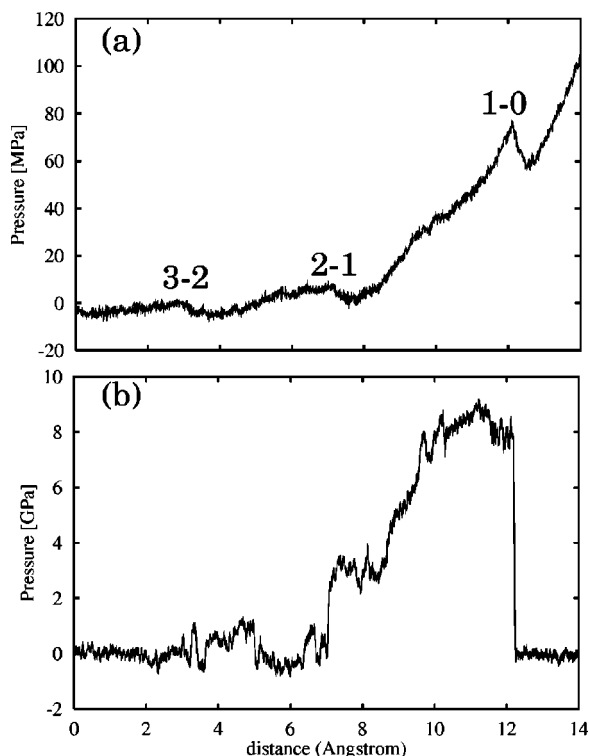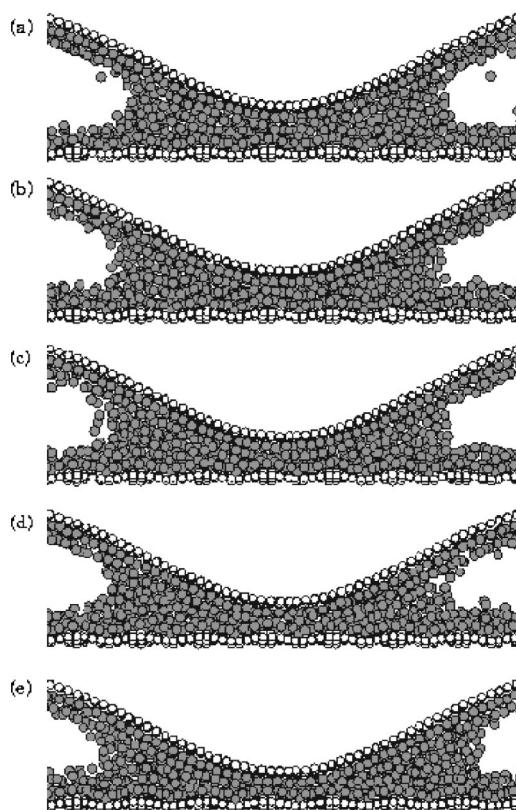

FIG. 18. Snapshot pictures for the approach of a Gaussian tip towards a rough substrate at the velocity $v_z = 1$ m/s. The snapshot pictures correspond to the block displacements (a) 0.22, (b) 1.22, (c) 2.22, (d) 3.22, and (e) 4.72 Å. The figure shows the central 80 Å×20 Å section (in the xy-plane) of the contact area. Note that the disordered (fluid-like) structure in the contact region is considerable in cases (a)–(d). In case (e), we have some layering, but the in-plane disorder is still maintained (see also Fig. 19).

Figure 23 shows snapshot pictures of the last lubricant layer during squeeze-out, after removing the block and substrate atoms. The figure contains xy projection of horizontal slices of the layer of lubricant molecules (polymeric chains) closest to the substrate. The distance the upper surface of the block has moved towards the bottom surface of the substrate is indicated for each snapshot picture. We note that the size of the $C_{16}H_{34}$-domains (areas of aligned polymeric chains) increases during the squeeze process (compare snapshots at $d=0$ and 22 Å)—the system require a ''long'' time in order to form large ordered domains. A certain realignment of polymeric chains inside domains and deformations of domain boundaries is seen during the squeeze-out of the last layer of lubricant molecules. We note that in the initial state of the nucleation of the squeeze-out, some polymer chains in the vicinity of the nucleation region, were not strictly localized to one layer (top or bottom layer) but spanned between the the first and the second layers.

Figure 24 shows the evolution of the shape of the block-asperity during squeezing ($v_z = 5$ m/s) and sliding ($v_x = 10$ m/s). Note that at short block–substrate separation the shape of the block becomes asymmetric. A detailed study shows that the block distorts upwards on the entrance (or inlet) side (the left hand side in the figure) while it distorts downwards on the exit side (the right hand side). This is exactly the result predicted by elastohydrodynamics, al-
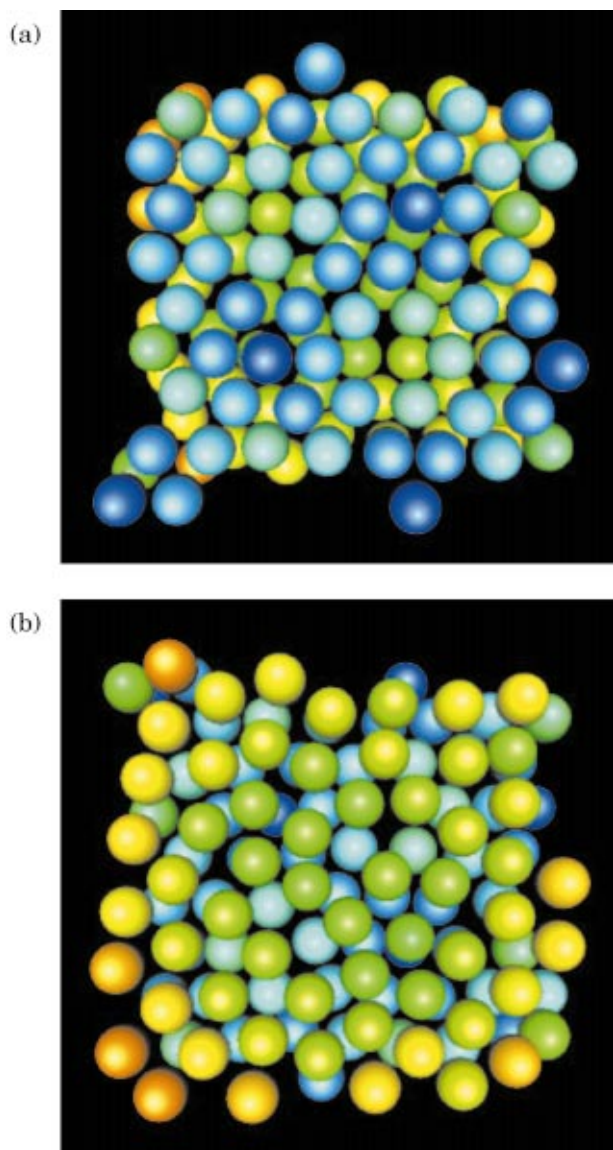

FIG. 17. The variation of (a) the average pressure, (b) the pressure at a specific central atom, as a function of the displacement of the upper surface of the block towards the (rough) substrate. The n-m labels stands for the layering transition from n to m layers. Squeezing velocity $v_z = 1$ m/s.

J. Chem. Phys., Vol. 117, No. 8, 22 August 2002

Phenomenology of squeezing and sliding   3909

(a)

(b)

FIG. 19. (Color) Snapshot pictures of the CH_4 atoms in the contact area for a block coordinate 4.72 Å. It shows two lubrication layers confined between the block asperity and a rough substrate (solid Au atoms are excluded). The figure is centered at the center of the contact area, revealing 30 Å $\times$ 30 Å (in the xy-plane). The color scheme represents the vertical z-coordinate, changing from dark blue at the first layer next to the substrate to red far away. (a) is from the substrate side and (b) from the block side. Both layers exhibit an in-plane disorder.

though the present lubrication film is too thin for this theory to be strictly valid. In elastohydrodynamics, the effect comes about because of the viscosity of the liquid: according to hydrodynamics there will be a higher pressure in the lubricant on the entrance side than on the exit side, and this will distort the elastic walls in the way outlined above. Note also that the nucleation of the squeeze out in the last snapshot picture is closer to the exit side than to the entrance side, again as expected from elastohydrodynamics. During squeezing (without sliding) the block shape remains symmetric.

Finally, let us present results for another $C_{16}H_{34}$–wall system. We assume that the block wall has a cosine corrugation (as in the case of Xe studied above), and that a $C_{16}H_{34}$
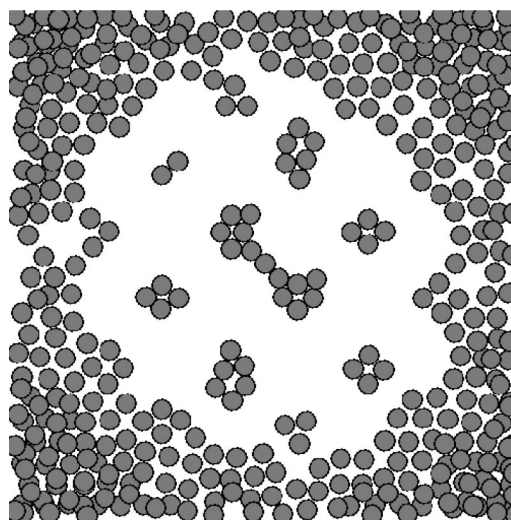

FIG. 20. Simulation snapshot of lubricant atoms for the case of a rough substrate. The figure shows trapped lubricant atoms, left after the (partial) squeeze-out of the last monolayer (top view; solid atoms are excluded).

bead unit interacts with the solid walls with the same parameters as for Xe. The substrate lattice spacing is 3.25 Å and the block lattice spacing is 2.89 Å.

Figure 25 shows the squeeze-out behavior of this system. Shown is the dependence of (a) the average pressure and (b) the average $C_{16}H_{34}$ kinetic energy, on the distance the upper surface has moved towards the substrate. The temperature $T = 300$ K, and the squeeze velocity $v_z = 2$ m/s. Note the well defined layering transitions, similar to the layering transitions observed for incommensurate layers of Xe in Ref. 7.

In Fig. 26 we show a snapshot picture (from the central region of the contact area) at the end of the squeeze-out in Fig. 25, but after reducing the squeeze pressure to 0.1 GPa, where the system has a single monolayer of molecules trapped in the contact region. Note that most of the $C_{16}H_{34}$ chains are lined up along the squeeze-out direction ($\pm x$-direction). Note also the "defect" in the center of the
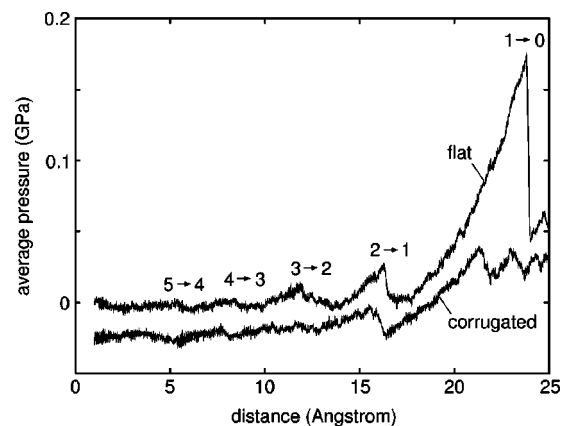

FIG. 21. The dependence of the average pressure on the distance by which the upper surface of the block has moved towards the bottom surface of the substrate. Results are shown both for a "flat" substrate, and for a substrate with short-wavelength corrugation (see the text). The curve for a corrugated substrate is displaced (for clarity) towards negative pressure by 0.02 GPa. The transitions from $n \rightarrow n-1$ monolayers of $C_{16}H_{34}$ are indicated. Squeeze velocity was $v_z = 2$ m/s.
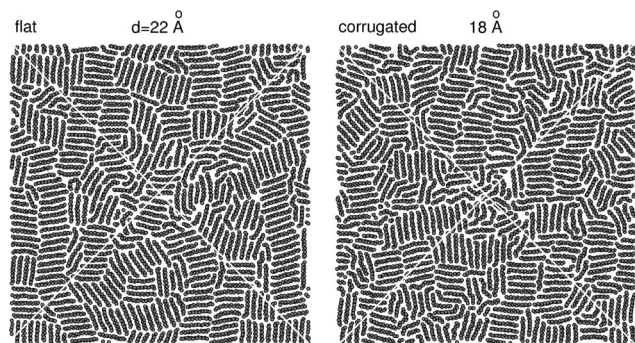
FIG. 22. Snapshot pictures of $C_{16}H_{34}$ monolayers adsorbed on the substrate for the flat (left image) and corrugated (right image) substrate, immediately before the nucleation of squeeze-out. The distance by which the upper surface of the block has moved towards the bottom surface of the substrate is indicated for each snapshot. Squeeze velocity was $v_z = 2$ m/s.

contact region where one polymer chain crosses another polymer chain; this defect was very stable, prevailing also during sliding.

IV. SIMULATION RESULTS: SLIDING

We now present results of MD-sliding friction simulations at a constant load, which is an external vertical force acting on the block, included in the equation of motion for the block. We have performed sliding friction simulations for Xe and $C_{16}H_{34}$ lubrication films. In this section we present some of these results. Consider first the system shown in Fig. 26. We have performed sliding friction studies for this system at the average pressure $P = 0.1$ GPa, starting with the
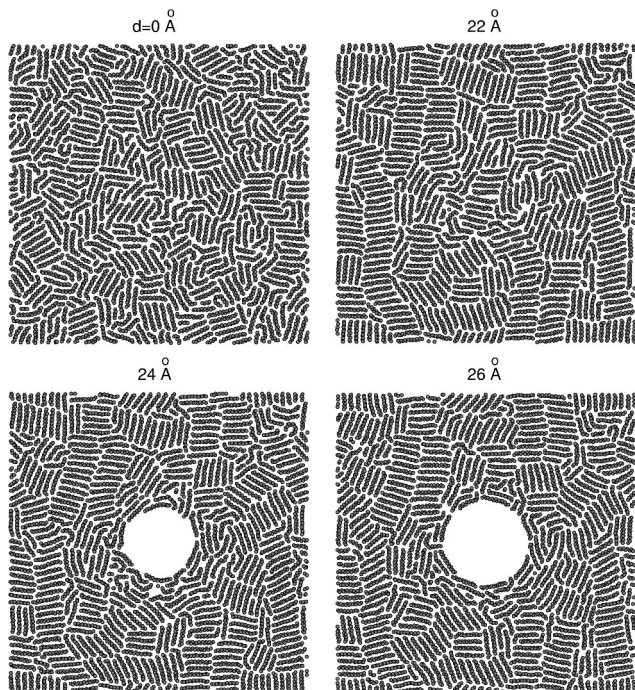

FIG. 23. Snapshot pictures (for different block positions d) of the lubricant layer during squeeze-out, after removing the block and substrate atoms. xy projection of a horizontal slice (xy-plane, $-3 \text{ Å} < z < 5 \text{ Å}$) showing the layer of $C_{16}H_{34}$ molecules closest to the substrate. Squeeze velocity $v_z = 2$ m/s.
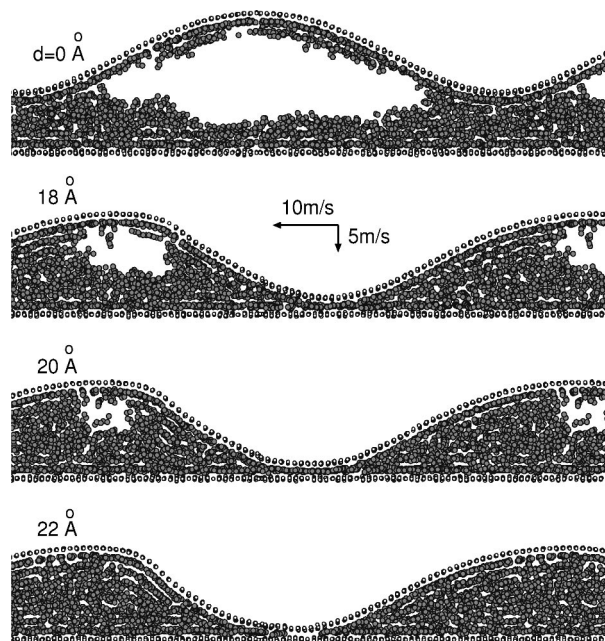

FIG. 24. Snapshot pictures during squeeze-out and sliding. Vertical slice (xz-plane, $-10 \text{ Å} < y < 10 \text{ Å}$). The distance d by which the upper surface of the block has moved towards the bottom surface of the substrate is indicated for each snapshot. A corrugated substrate is used here, with sliding velocities $v_z = 5$ and $v_x = 10$ m/s. The evolution of the shape of the block towards an asymmetric shape is clearly seen.

configuration shown in Fig. 26. In these simulations the block, whose mass was taken 10^6 atomic units (hydrogen mass), was pulled by a spring with the spring constant $k_s = 3$ N/m. This is the same spring constant as in our earlier study of sliding dynamics with a Xe lubricant.[8] In this latter case we observed stick–slip motion when the spring velocity decreased below ~ 10 m/s. In the present case, no stick–slip motion is observed even when the spring velocity is decreased to 0.42 m/s. We attribute this to much longer rearrangement times of the $C_{16}H_{34}$-system, so that the strengthening of the static friction force with the time of stationary contact is negligible on the time scale of the simulations.[19–22] This is related to the nature of the transition from stick to slip: in the present case there is only a small change in the adsorbate structure (small local displacement during the elastic-instability transion) while for the Xe-system studied in Ref. 8 the adsorbate layer underwent a phase transformation from a domain wall super structure at stick to an incommensurate (hexagonal) structure at slip. Another consequence of this fact is the observation that the static friction coefficient nearly equals the (low velocity) kinetic friction coefficient, $\mu_s \approx \mu_k$, while for the Xe-system it was found that $\mu_s \approx 4\mu_k$.[8] Figure 27 shows the kinetic friction coefficient as a function of the logarithm (with 10 as the basis) of the sliding velocity v. Note that $\mu(v) \rightarrow 0.0135$ as $v \rightarrow 0$. Of course, for very low sliding velocity we expect thermally activated creep to manifest itself, and $\mu(v)$ will then decrease with decreasing v, but these low sliding velocities cannot be probed in the computer simulations.

Figure 28 shows the time dependence of μ when starting from equilibrium at $t = 0$, with the free end of the spring moving with velocity of 3.4 m/s for $t < 600$. At $t = 600$ we

J. Chem. Phys., Vol. 117, No. 8, 22 August 2002

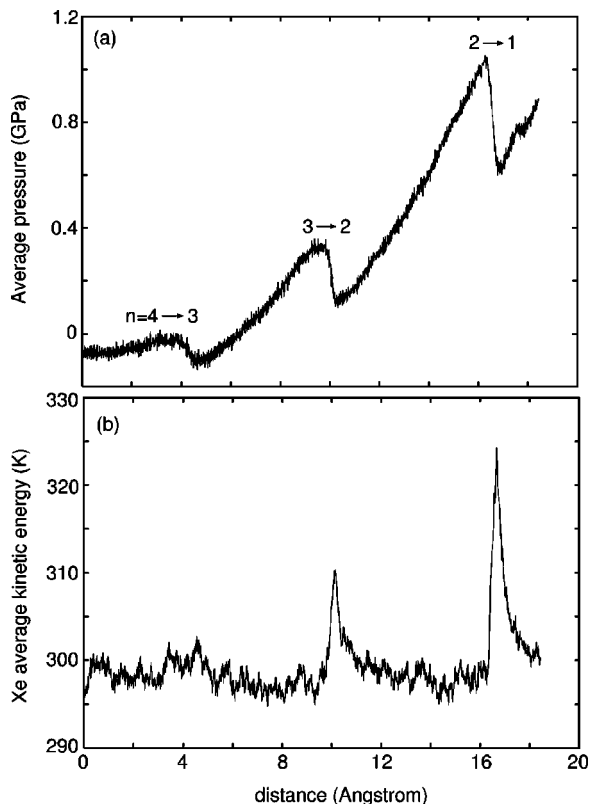Phenomenology of squeezing and sliding   3911

FIG. 25. The dependence of (a) the average pressure and (b) the average $C_{16}H_{34}$ kinetic energy on the distance the upper surface has moved towards the substrate. The squeeze velocity is $v_z = 2$ m/s.

FIG. 27. The kinetic friction coefficient as a function of the logarithm (with 10 as the basis) of the sliding velocity v. The normal (average) pressure $P = 0.1$ GPa.

abruptly decrease the pull velocity to 0.42 m/s. Note that *atomic stick–slip oscillations* occur. These oscilations are independent of the external spring constant k_s: during the stick time period elastic energy is stored up in the system and during the slip time period this energy is dissipated in a rapid event where the block moves forwards a single lattice con-

stant. This type of atomistic stick–slip motion has often been observed with the friction force microscopy.

We have found that the friction force remains finite as the sliding velocity $v \to 0$ (see Fig. 27). This can only be the case if rapid processes occur at the interface even when v is arbitrary small. Thus, at very low sliding velocity, events of (slow) elastic loading followed by very rapid slip or yield occurs at the interface. A similar effects occur during plastic deformation of a solid. In general, the slip or yield events will not occur simultaneously over the whole contact area, but local stick–slip events may occur at the interface resulting in small local forward displacement of the surfaces areas at the interface. This type of local motion is possible only when the elastic properties of the solid walls are taken into account in the analysis. In computer simulations (like the ones discussed above), where the contact area is much smaller than in most practical situations, the elementary slip events usually involve the whole contact area.
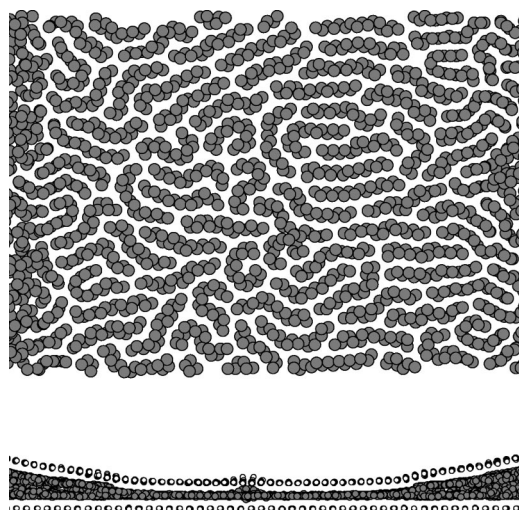

FIG. 26. Snapshot picture of the central region of the monolayer lubrication film from the end of the squeeze-out in Fig. 25. (a) Top view without block and substrate atoms. (b) Side view of a wider region of the contact area than in (a) and with the substrate and block atoms included.
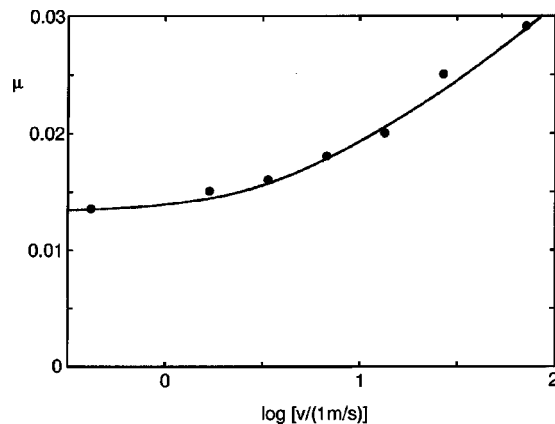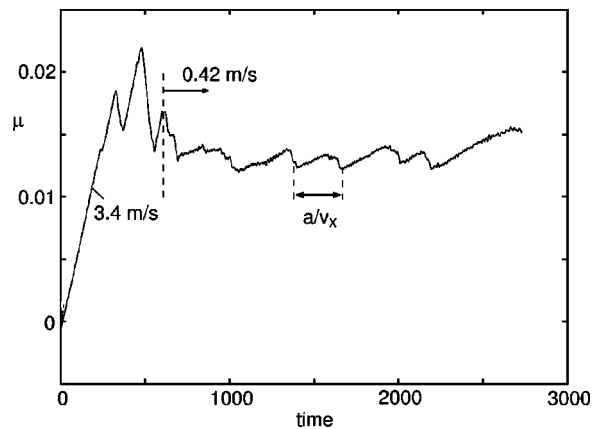

FIG. 28. The time dependence of μ after starting from equilibrium at $t = 0$, with the free end of the spring moving at a velocity of 3.4 m/s for $t < 600$. At $t = 600$ we abruptly decrease the pull velocity to 0.42 m/s. The normal (average) pressure equals $P = 0.1$ GPa. At the sliding velocity $v_x = 0.42$ m/s the time period $\Delta t \approx 260$ corresponds to the displacement of one substrate lattice constant.

3912   J. Chem. Phys., Vol. 117, No. 8, 22 August 2002

Persson *et al.*

In the system studied above atomic stick–slip has been observed during steady sliding. A visual inspection of the monolayer lubrication film did not display any major changes in the film structure during the elementary (atomic scale distance) stick–slip–stick event. This is in sharp contrast to an earlier study with a monolayer of Xe as a lubricant,[8] where again we observed that during steady sliding (at low sliding velocity) the lubricant film performed atomic distance stick–slip motion, but in contrast to the $C_{16}H_{34}$ case, during each slip event the whole monolayer film in the high-pressure contact region changed from a domain wall super structure (at stick) to an incommensurate hexagonal solid structure during slip. Another, already mentioned difference is that while for the present $C_{16}H_{34}$ sliding system the static friction coefficient nearly equals the (low-velocity) kinetic friction coefficient, $\mu_s \approx \mu_k$, for the Xe case $\mu_s \approx 4\mu_k$. For the Xe system we observed that at low sliding velocity the slip is mainly localized to one of the lubrication–wall interfaces. We found a similar effect also for the present $C_{16}H_{34}$ system.

The results discussed above were for perfect crystaline solids walls, with no defects or surface roughness. In almost all practical applications, the solid walls will be rough and, in particular, have atomic scale roughness such as steps or strongly bound adatoms. This may have a profound influence on the microscopic processes in the lubrication film during slip. Thus, for example, steps or adatoms may give rise to pinning of patches of the lubrication film so that during sliding strong 2D-plastic deformation may occur within the lubrication film as different areas (pinned to different walls) of the film moves relative to other areas. Thus, when a point defect or steps are introduced on the solid walls, the (nearly perfect) incommensurate solid state observed for Xe during slip (see Ref. 8) is likely to be replaced by a liquid-like or disordered state. This effect has, in fact, been observed in earlier model studies[23] where a very low concentration of point defect converted a sliding incommensurate Xe layer to a 2D liquid-like state. A similar effect has been observed recently by Gao *et al.*[2] during shear of molecular thin $C_{16}H_{34}$ films (~4 monolayers) between atomically rough solid walls. For smooth walls the lubricant film was in a solid-like state and a large wall–lubricant slip was observed, while for *atomically rough* surfaces they observed that, for a 4 monolayer $C_{16}H_{34}$ film, the monolayers in direct contact with the solid walls were strongly pinned to the walls, while the remaining 2 monolayers exhibited liquid-like behavior during shear and squeezing.

An additional indication that atomic scale surface roughness may be of great importance in sliding friction comes from a study of the magnitude of the kinetic friction coefficient. Experimentally, for boundary lubricated surfaces one have typically $\mu_k \approx 0.1$, which is ~10 times larger than observed in most molecular dynamics studies with smooth surfaces. Thus, for the $C_{16}H_{34}$ lubricant in Fig. 27 (monolayer coverage, average normal pressure 100 MPa) we have found the low-velocity kinetic friction coefficient to be $\mu \approx 0.014$. Gao *et al.*[2] found $\mu \approx 0.01$ for the same lubricant but under drastically different conditions (four monolayers, normal pressure 50 MPa). For the Xe-lubricant system studied in
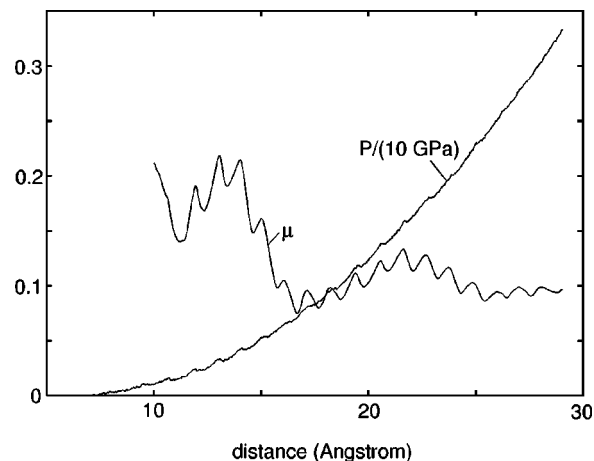

FIG. 29. The friction coefficient μ and the (average) pressure P as a function of the distance the upper surface of the block has moved towards the bottom surface of the substrate. The squeezing velocity $v_z = 4.6$ m/s and the sliding velocity $v_x = 18.3$ m/s. The lubricant film thickness change from ~4 Xe monolayers to a single Xe monolayer during the squeeze process. Note that as the pressure P increases from 0.5 GPa to 3.5 GPa the friction coefficient fluctuate only between $\mu = 0.1 \pm 0.02$. Adapted from Ref. 7.

Ref. 8 we found $\mu \approx 0.01$. These values are all much smaller than typically observed experimentally. This could be explained by assuming that in real systems the molecule–wall interaction potential has a much larger (atomic) corrugation than used in all the simulations (see below). However, we believe that a more likely explanation is the occurrence of atomic scale roughness (e.g., steps) on the solid walls, which, as discussed above, gives rise to a strong pinning and, during sliding, "plastic deformation" in the lubrication film.[24] In this way much more energy will be "dissipated" per unit distance of sliding giving rise to a strong enhancement in the friction coefficient as indeed observed by Gao *et al.*[2] for rough solid walls.

Commensurate adsorbate layers are usually strongly pinned. In Ref. 7 we study a case where the block and substrate lattice spacing was nearly the same as the natural Xe–Xe distance. In this case a strongly pinned 1×1 Xe-structure was formed. Starting with a 4 monolayer Xe film, we were not able to squeeze out any Xe by just increasing the squeezing pressure. However, during squeezing and sliding we were able to squeeze out most of the Xe. In this case we observed that the kinetic friction coefficient was of order 0.1 (see Fig. 29), as observed in most boundary lubrication experiments. This is in sharp contrast to most other studied cases, were weakly pinned (incommensurate) structures are formed and where $\mu_k \approx 0.01$. As discussed above, we believe that the origin of this discrepancy is that most real surfaces have a high concentration of defects (e.g., steps), which tend to give rise to strong pinning of the first adsorbed layers, similar to the formation of commensurate structures. We emphasize that only in improbably accidental cases will the natural spacing between the lubricant molecules be similar to the lattice constant of the block or the substrate, so that in most cases pinning by defects seems necessary in order to explain the observation of $\mu \approx 0.1$. We should point out, however, that we have often observed that the high-presssure
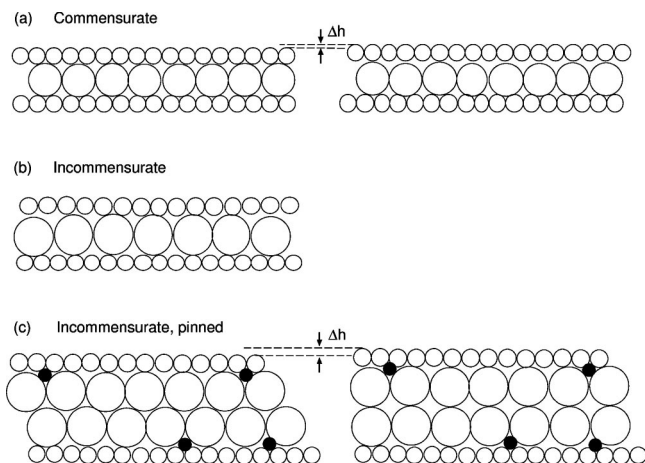
FIG. 30. Left: (a) Commensurate, (b) incommensurate and (c) pinned incommensurate adsorbate layers between two solid walls. Right: During sliding the spacing between the solid walls must expand by Δh. The expansion is large for cases (a) and (c) but very small in case (b).

FIG. 31. The onset of slip occur via the propagation of a frictional shear crack.

at the interface squeeze the lubrication atoms into a structure which is commensurate with respect to one of the solid walls (block or substrate), even if the resulting nearest neighbor spacing between the atoms is far away from the "natural" distance.

In the study presented in Ref. 7 the kinetic friction coefficient was nearly independent of the perpendicular squeezing pressure (see Fig. 29) at high enough pressure. This effect seems to be very general, and in fact has been known for many years, e.g., early work by Bowden and Tabor showed that the shear stress in most cases is nearly proportional to the local pressure in the contact areas. For example, if one compares the friction properties of lubricated tin surfaces (hardness ~ 70 N/m^2) with lubricated hard steel surfaces (hardness ~ 7000 N/m^2), the friction coefficient typically differ by less than a factor of 2, in spite of the fact that the local pressure in the tin contact areas is ~ 100 times less than for the steel surfaces. Such a pressure independence of the kinetic friction coefficient can be understood based on the following microscopic picture: during sliding molecular groups at the interface flip from one configuration to another. The flips are accompanied by local expansions of the system. The barrier to slide will have a contribution from the work done against the external pressure P during the local expansions. This effect has been emphasized and discussed by Israelachvili and coworkers and a lucid discussion is presented in Ref. 25.

Figure 30(a) shows a case where, at stick, a monolayer lubrication film forms a commensurate structure between two solid walls. At slip the spacing between the solid walls at the interface must expand by a distance Δh. For an incommensurate layer [see Fig. 30(b)] no, or very small, expansion is nececessary, i.e., $\Delta h \approx 0$. However, for two incommensurate lubricant layers pinned by defects or surface roughness to the solid walls [the pinning centers are denoted by black dots in Fig. 30(c)] a large expansion Δh may occur at the onset of slip. The energy necessary in order to start slip will be
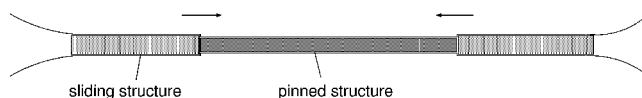
$$E = N \Delta E + PA \Delta h,$$

where N is the number of lubrication molecules, and ΔE the (average) change in the lubricant–wall and lubricant–lubricant interaction energy between the onset of slip and the "ground state" in the absence of an applied shear stress. We can estimate the static friction using

$$A \sigma_s b/2 \approx N \Delta E + PA \Delta h,$$

where b is the interfacial displacement distance at the onset of slip, and σ_s is the shear stress necessary to initiate sliding. Thus,

$$\sigma_s \approx 2n_a \Delta E/b + 2P \Delta h/b,$$

and the static friction coefficient $\mu_s = \sigma_s/P$:

$$\mu_s \approx 2n_a \Delta E/(bP) + 2 \Delta h/b.$$

For the Xe system considered in Ref. 8 the amplitude of the height fluctuation as a single Xe atom is displaced between a hollow and a bridge site is $\approx 0.04a$ (where a is the lattice constant of the cubic walls). With $b \approx a/2$ and $\Delta h \approx 0.04a$ we get $2 \Delta h/b \approx 0.16$, which is nearly three times larger than the result for the static friction coefficient observed in the computer simulation $\mu_s \approx 0.06$. However, a detailed study of snapshot pictures of the adsorbate layer during the transition from stick to slip showed that the slip started at the periphery of the contact area and propagated rapidly towards the center of the contact area (see Fig. 31); we may denote this as a frictional shear crack. Since the shear stress at the crack-edge is enhanced from the uniform value assumed above, it is clear that the transition from stick to slip will occur at a lower shear stress than predicted by the theory above. This effect will be even more important for a larger contact area (as occurs in most practical applications and also in Surface Forces Apparatus measurements). We note also that the ground state Xe-structure in Ref. 8 (a domain wall super structure) does not have all the Xe atoms (in the high-pressure region) in hollow sites, so that the change in Δh may be smaller than calculated above, which would be consistent with a smaller μ_s-value.

A Coloumbs friction law state that the friction force is proportional to the normal load. He, Müser and Robbins[26] (and others) have suggested that the explanation for this fact is the (approximate) independence of the friction coefficient on the normal pressure, which always is the case at large enough pressure (see above). However, we do not believe that this is the correct explanation in most practical applications, but rather it follows from the fact that for rough surfaces the area of real contact is proportional to the load, and the pressure distribution in the area of real contact is independent of the load.[27,28]

V. SUMMARY AND CONCLUSION

We have studied the properties of Xe, CH_4 and $C_{16}H_{34}$ lubricant confined between two approaching solids. The model accounts for the curvature and elastic properties of the solid surfaces. We considered both smooth surfaces, and surfaces with short-scale roughness. In most cases we observed well defined molecular layers develop in the lubricant film when the width of the film is of the order of a few atomic diameters, but in some cases atomic scale roughness inhibit the formation of these layers, and the lubrication film exhibits liquid-like properties. We observed that an external squeezing-pressure induced discontinuous, thermally activated, changes in the number n of lubricant layers.

The most important results are the following: (1) It is shown that the layering transition tends to nucleate in disordered or imperfect regions in the lubrication film. (2) The squeeze process is acompanied by phase transformations in the high-pressure region, which allows the confining surfaces to come closer and lower the elastic energy. (3) Surface roughness hinders the formation of solid-like lubricant structures and liquid-like (disordered) layers are observed. This in turn leads to a reduction in the squeeze-out pressure.

These observations also suggest a new explanation to recent intriguing observations by Raviv *et al.*,[29] showing that water exhibits fluid-like behavior down to the last confined monolayer. When water freezes its volume increases and thus solidification is accompanied by an energetic penalty in terms of elastic energy, making it unfavorable.

[1] B. N. J. Persson, *Sliding Friction: Physical Principles and Applications* (Springer-Verlag, Heidelberg, 2000); Surf. Sci. Rep. **33**, 83 (1999); J. Krim, Sci. Am. **275**, 74 (1996); S. Granick, Phys. Today **57**, 26 (1999).

[2] J. Gao, W. D. Luedtke, and U. Landman, Tribol. Lett. **9**, 3 (2000).

[3] J. Gao, W. D. Luedtke, and U. Landman, Phys. Rev. Lett. **79**, 705 (1997); J. Phys. Chem. B **101**, 4013 (1997).

[4] J. N. Israelachvili, *Intermolecular and Surface Forces* (Academic, London, 1995); M. L. Gee, P. M. McGuiggan, and J. N. Israelachvili, J. Chem. Phys. **93**, 1895 (1990).

[5] L. Demirel and S. Granick, Phys. Rev. Lett. **77**, 2261 (1996); J. Chem. Phys. **109**, 6889 (1998).

[6] J. Klein and E. Kumacheva, Science **269**, 816 (1995); J. Chem. Phys. **108**, 6996 (1998); **108**, 7010 (1998).

[7] B. N. J. Persson and R. Ballone, J. Chem. Phys. **112**, 9524 (2000).

[8] B. N. J. Persson, J. Chem. Phys. **113**, 5477 (2000).

[9] B. N. J. Persson and E. Tosatti, Phys. Rev. B **50**, 5590 (1994).

[10] F. Mugele and M. Salmeron, Phys. Rev. Lett. **84**, 5796 (2000).

[11] S. Zilberman, B. N. J. Persson, A. Nitzan, F. Mugele, and M. Salmeron, Phys. Rev. E **63**, 055103 (2001).

[12] S. Zilberman, B. N. J. Persson, and A. Nitzan, J. Chem. Phys. **115**, 11268 (2001).

[13] J. N. Israelachvili (private communication).

[14] W. l. Jorgensen, J. D. Madura and C. J. Swenson, J. Am. Chem. Soc. **106**, 6996 (1984).

[15] T. K. Xia, J. Ouyang, M. W. Ribarsky, and U. Landman, Phys. Rev. Lett. **69**, 1967 (1992).

[16] D. K. Dysthe, A. H. Fuchs, and B. Rousseau, J. Chem. Phys. **112**, 7581 (2000).

[17] M. P. Allen and D. J. Tildesley, *Computer Simulations of Liquids* (Clarendon, Oxford, 1989).

[18] Note in Fig. 17(b) that the local pressure at the center drops to zero after the $n=1\rightarrow0$ transition. It is a local effect, coming from the fact that there are no lubricant atoms in the vicinity of the center block atom, and it resides on top of a roughness valley in the substrate, such that its interaction with the substrate is very weak.

[19] O. M. Braun and J. Röder, Phys. Rev. Lett. **88**, 096102 (2002).

[20] M. G. Rozman, M. Urbakh, J. Klafter, and F. J. Elmer, J. Phys. Chem. **102**, 7924 (1998).

[21] T. Baumberger, C. Caroli, and O. Ronsin, Phys. Rev. Lett. **88**, 075509 (2002).

[22] B. N. J. Persson and V. L. Popov, Solid State Commun. **114**, 261 (2000).

[23] B. N. J. Persson, J. Chem. Phys. **103**, 3849 (1995).

[24] B. N. J. Persson, Phys. Rev. B **51**, 13568 (1995).

[25] J. Israelachvili, *Fundamentals of Tribology and Bridging the Gap between the Macro- and Micro/Nanoscales*, edited by B. Bushan (Kluwer, Dordrecht, 2001), pp. 631–650.

[26] G. He, M. H. Müser, and X. Robbins, Science **284**, 1650 (1999).

[27] J. A. Greenwood and J. B. P. Williamson, Proc. R. Soc. London, Ser. A **295**, 300 (1966).

[28] B. N. J. Persson, Phys. Rev. Lett. **87**, 116101 (2001).

[29] U. Raviv, P. Laurat, and J. Klein, Nature (London) **413**, 51 (2001).